UNIVERSIDADE DA BEIRA INTERIOR
Ciências da Saúde

Desenvolvimento de nanomateriais para a terapia fototermal do cancro

Cleide Isabel Pais Silva

Dissertação para obtenção do Grau de Mestre em
Ciências Biomédicas
(2º ciclo de estudos)

Orientador: Professor Doutor Ilídio Joaquim Sobreira Correia
Co-orientador: Mestre Duarte Miguel de Melo Diogo

Covilhã, outubro de 2016

“Do you wish to rise? Begin by descending.
You plan a tower that will pierce the clouds?
Lay first the foundation of humility.”

Saint Augustine

À minha avó, mãe e pai, por tornarem tudo possível.

Acknowledgements

Just for today, be grateful.

First of all, I would like to acknowledge my supervisor, Professor Ilídio Correia, for the possibility to integrate his group and to develop my master thesis with them. His orientation, expertise and wise advices throughout this year were crucial to accomplish this work. He made me improve and surpass myself, either at the professional and personal level, and I am likewise grateful to him for that. I am also deeply thankful to Duarte Diogo, my co-supervisor, for his guidance, for believing in me and in my work and for always keeping me motivated. The constant discussion of ideas and the know-how he transmitted to me contributed to my growth as a researcher. All his support made the development of this work easier.

I also thank Diana Dias, Elisabete Costa and Marco Carvalho, not only for their accompaniment and help during the long lab protocols, but mainly for their friendship, talks and laughs. To my lab partners, I thank their fellowship and moments of conviviality. To all, I wish the best.

To my family, there is no word that expresses how grateful I am. Foremost, I profoundly thank my mom, my all-time guide, for the endless encouragement, belief, prudent advices and love. To my father, I acknowledge his attention and trust, which I assume his silence hides. I thank my brother for his affection, concern and for always having faith in its "little princess". To my lovely and brave grandmother, the cornerstone of the family, I address an enormous thank for the encouragement and for being an inspiration to me. To all of you, thank you, thank you from the bottom of my heart.

To Telmo, my longtime friend, I thank for our daily talks, support and for never giving up on our friendship. "Out of the sight, close to the heart".

Last, but not least, words cannot express how extremely grateful I am to my boyfriend, Davide, for his continuous support, comprehension and endless love throughout these years. Most of all, I have to recognize the unconditional patience over this last year, that made every single day seems easier. Just for today… I am grateful for having you by my side.

Thank. A little word with so much meaning.

Thank you all.

Resumo

O cancro da mama é um dos mais prevalentes e uma das principais causas de morte das mulheres em todo o mundo. No caso específico da população Portuguesa, as taxas de incidência e mortalidade associadas ao cancro da mama têm vindo a aumentar nos últimos anos. Este cenário deve-se maioritariamente à ineficácia dos tratamentos atualmente disponíveis (cirurgia, radioterapia e terapias baseadas em pequenas moléculas), cuja eficácia terapêutica é reduzida devido a problemas de segurança, toxicidade não específica e ainda devido aos mecanismos de resistência a fármacos que as células cancerígenas apresentam. Estes factos evidenciam a necessidade de desenvolver novas abordagens terapêuticas.

Nas últimas décadas, as fototerapias têm sido investigadas como estratégias alternativas para combater as células cancerígenas. Estas modalidades terapêuticas incluem a terapia fotodinâmica e a fototérmica. Ambos os tratamentos dependem da irradiação da região tumoral com radiação com um comprimento de onda próximo do infravermelho (near-infrared (NIR)) que ativa moléculas fotoresponsivas, as quais induzem a produção de espécies reativas de oxigénio (terapia fotodinâmica) ou um aumento de temperatura (terapia fototérmica), que têm um efeito citotóxico nas células cancerígenas. Porém, estes tratamentos ainda têm que ser otimizados para incrementar a sua eficácia e seletividade para o tumor.

A nanotecnologia tem permitido ultrapassar algumas das principais limitações da aplicação das fototerapias no tratamento do cancro, através da encapsulação de agentes fotoresponsivos em nanopartículas. A encapsulação de moléculas fotoresponsivas à luz NIR em nanoveículos é crucial para reverter a baixa solubilidade destas moléculas em fluidos biológicos. Para além disso, estes nanotransportadores acumulam-se preferencialmente no tumor devido às suas propriedades físico-químicas, o que permite aumentar a biodisponibilidade das moléculas fotoresponsivas encapsuladas nestes, melhorando assim a eficácia e seletividade destas abordagens terapêuticas.

Na presente tese é descrito o desenvolvimento de um nanoveículo com capacidade de encapsular um agente fotoresponsivo à luz NIR, para aplicação na fototerapia do cancro da mama. Para tal, foram utilizados dois derivados de vitamina E, succinato de D-α-tocoferil polietilenoglicol 1000 (TPGS) e succinato de D-α-tocoferil (TOS), para formular micelas anfifílicas com uma estrutura tipo "núcleo-concha". O TPGS e o TOS foram selecionados por apresentarem atividade anticancerígena intrínseca (por exemplo, através da produção de espécies reativas de oxigénio) e pela sua capacidade para encapsular moléculas pouco solúveis em água. O iodeto de 2-[2-[2-cloro-3-[(1,3-dihidro-3,3-dimetil-1-propil-2H-indol-2-ilideno) etilideno]-1-ciclohexeno-1-il]etenil]-3,3-dimetil-1-propilindólio (IR780) foi escolhido devido à sua versatilidade como molécula fotoresponsiva, uma vez que possui características que

permitem a sua aplicação como agente fototerapêutico (terapia fotodinâmica e fototermal) e de diagnóstico. No presente estudo foram obtidas micelas de TPGS-TOS contendo IR780 (IR780-TTM) com características físico-químicas adequadas, utilizando proporções de TPGS e TOS específicas aquando da sua formulação. As micelas produzidas permitiram a encapsulação do IR780 com elevada eficiência. Nos ensaios *in vitro* realizados verificou-se que as IR780-TTM medeiam um efeito citotóxico nas células cancerígenas após irradiação com luz NIR, através da produção de espécies reativas de oxigénio (terapia fotodinâmica). Esta eficiente ablação das células cancerígenas foi alcançada usando uma concentração de IR780 mais baixa do que a que foi descrita até agora na literatura. Aliado a isto, constatou-se que as IR780-TTM demonstram potencial para serem utilizadas como agentes de fototermia e imagiologia.

Em suma, os nanoveículos desenvolvidos na presente tese apresentam um enorme potencial para a terapia fotodinâmica do cancro da mama. Por outro lado, as propriedades fototérmicas e imagiológicas que as IR780-TTM apresentam aumentam a aplicabilidade destas micelas no tratamento e diagnóstico do cancro.

Palavras-chave

Cancro da mama, IR780, micelas de TPGS-TOS, terapia fotodinâmica, terapia fototérmica.

Resumo alargado

Na atualidade, o cancro é um dos principais problemas de saúde pública que afeta a população a nível mundial. Em particular, o cancro da mama é uma das neoplasias mais comuns e com maior taxa de mortalidade entre o sexo feminino. Este cenário deve-se essencialmente à ineficiência das terapias anticancerígenas convencionais, uma vez que as moléculas terapêuticas apresentam problemas intrínsecos, como sejam a baixa solubilidade, fraca disponibilidade no local do tumor e acumulação não específica em tecidos saudáveis. Por outro lado, o desenvolvimento de mecanismos de resistência a fármacos por parte das células cancerígenas causa também efeitos adversos para o paciente. Todos estes factos evidenciam a necessidade urgente de desenvolver novas terapias anticancerígenas.

Neste contexto, as terapias fotodinâmica e fototérmica têm-se revelado como alternativas promissoras para o tratamento do cancro. Estas abordagens terapêuticas exploram a aplicação de radiação com comprimento de onda próximo do infravermelho (near-infrared (NIR); 750-1000 nm) na região tumoral para ativar moléculas fotoresponsivas, o que se traduz na formação de espécies reativas de oxigénio (terapia fotodinâmica) ou num aumento de temperatura (terapia fototérmica), que causam citotoxicidade às células cancerígenas. Porém, este tipo de terapias necessitam de melhorias no que diz respeito à sua seletividade para as células cancerígenas. Para além disto, estas moléculas são geralmente lipofílicas, o que limita a dose que pode ser administrada.

Na última década, os investigadores têm explorado a encapsulação de moléculas fotoresponsivas em nanotransportadores. Esta estratégia visa aumentar a solubilidade destas moléculas, bem como protegê-las da degradação. Para além disto, estes nanotransportadores, devido às suas dimensões, podem permitir uma acumulação preferencial no tecido tumoral. Desta forma, é possível submeter o tumor a espécies reativas de oxigénio e calor após irradiação dos nanotransportadores com radiação NIR.

Na presente tese desenvolveu-se um nanotransportador micelar para mediar a entrega de um composto fotoresponsivo à luz NIR a células cancerígenas do cancro da mama. Para tal, foram utilizados dois derivados de vitamina E, succinato de D-α-tocoferil polietilenoglicol 1000 (TPGS) e succinato de D-α-tocoferil (TOS), uma vez que apresentam atividade anticancerígena intrínseca (nomeadamente através da produção de espécies reativas de oxigénio) e a sua combinação em meio aquoso leva à formação de micelas com carácter anfifílico, o que permite a encapsulação de compostos lipossolúveis responsivos à luz NIR. O iodeto de 2-[2-[2-cloro-3-[(1,3-dihidro-3,3-dimetil-1-propil-2H-indol-2-ilideno)etilideno]-1-ciclohexeno-1-il]etenil]-3,3-dimetil-1-propilindólio (IR780) foi selecionado como agente fotoresponsivo a encapsular nas micelas de TPGS-TOS devido à absorção que apresenta a 780 nm, que possibilita a sua interação

com a luz NIR. Esta propriedade é de extrema importância, uma vez que a radiação NIR penetra mais profundamente nos tecidos e apresenta interações mínimas com os componentes biológicos. Além disto, o IR780 é um composto fotoresponsivo versátil, uma vez que é capaz de produzir espécies reativas de oxigénio e/ou variações de temperatura, quando irradiado com luz NIR. Por outro lado, a capacidade que o IR780 tem de emitir fluorescência, permite ainda a sua aplicação na deteção de tumores, isto é, imagiologia de tumores.

Durante a otimização do processo de formulação das micelas de TPGS-TOS contendo IR780 (IR780-TTM) foram testadas várias proporções de TPGS e TOS, e verificou-se que a utilização de uma percentagem de 40, 33 ou 25 de TPGS permite produzir micelas com propriedades físico-químicas adequadas para encapsular e entregar IR780 a células cancerígenas. Para além disto, verificou-se que as IR780-TTM possuem excelentes propriedades como agentes fototerapêuticos devido à sua alta absorção de radiação NIR. Aliado a este facto, observou-se que as IR780-TTM são capazes de produzir, quando irradiadas com radiação NIR, uma variação de temperatura de até 18 °C, o que demonstra o potencial destas micelas para serem usados em fototermia.

Nos ensaios *in vitro* constatou-se que as IR780-TTM são internalizadas pelas células de cancro da mama, o que é fundamental para aumentar a concentração de IR780 no interior das células, visto que o composto na sua forma livre tem uma baixa translocação para o espaço intracelular. Estes estudos permitiram ainda confirmar o potencial das IR780-TTM para serem usadas em aplicações imagiológicas. Os estudos de viabilidade celular permitiram verificar que a utilização combinada de radiação NIR e das IR780-TTM, encapsulando apenas 1.5 μg mL^{-1} de IR780, reduziu a viabilidade celular das células cancerígenas para 19 %. Nestas mesmas condições, as células tratadas com IR780-TTM, mas que não foram irradiadas, permaneceram viáveis, o que demonstra que a fototerapia mediada pelas IR780-TTM é extremamente eficaz. Em estudos subsequentes verificou-se que a fototoxidade mediada pelas IR780-TTM é induzida pela produção de espécies reativas de oxigénio (terapia fotodinâmica). Aliado a isto, a capacidade intrínseca do TPGS e do TOS para produzirem espécies reativas de oxigénio parece dar um contributo importante para esta eficiente ablação celular. Por fim, é importante salientar que o efeito fototerapêutico mediado pelas IR780-TTM foi alcançado usando a menor concentração de IR780 descrita até ao momento na literatura, o que atesta a eficácia e o potencial das micelas desenvolvidas.

Em suma, o sistema micelar desenvolvido apresenta um enorme potencial para ser utilizado na terapia fotodinâmica do cancro da mama. Além disso, a natureza versátil das IR780-TTM é fundamental para a sua futura aplicação como agentes fototérmicos e de diagnóstico.

Abstract

Breast cancer is one of the most prevalent and one of the leading causes of cancer-related deaths among women worldwide. In the specific case of the Portuguese population, breast cancer incidence and mortality rates increased in the past years. This scenario is mostly owed to the ineffectiveness of the currently available treatments (surgery, radiotherapy and small molecule-based therapies), whose therapeutic success is hindered by safety issues, non-specific toxicity and resistance mechanisms displayed by cancer cells to drugs. Such emphasizes the demand for a plethora of novel therapeutic approaches.

In the past decades, light-induced therapies have started to be investigated as alternative strategies to combat cancer. These treatment modalities comprise photodynamic therapy (PDT) and photothermal therapy (PTT). Both therapeutic approaches depend on the external irradiation of the tumor region with near-infrared (NIR) light for activating photosensitizers or photothermal agents, that lead to the generation of reactive oxygen species (ROS; in PDT) or to a temperature increase (in PTT), which have a cytotoxic effect on cancer cells. Yet, such treatments still need to be further improved in what concerns their efficacy and selectivity towards the tumor region.

Recently, the entrapment of NIR photoabsorbers in nanoparticles surpassed problems like the poor solubility of these molecules in biological fluids. Moreover, nanoparticles due to their physicochemical properties can display a preferential tumor accumulation, which is crucial for increasing the loaded NIR photoabsorbers bioavailability and ultimately the efficacy and selectivity of this therapeutic approach.

Herein, a novel nanovehicle loaded with a NIR dye aimed for breast cancer phototherapy was developed. To accomplish that, two vitamin E derivatives, D-α-tocopheryl polyethylene glycol 1000 succinate (TPGS) and D-α-tocopheryl succinate (TOS), were used to assemble amphiphilic micelles with a core-shell structure. TPGS and TOS were selected due to their intrinsic anticancer activity (e.g. through the generation of ROS) and ability to encapsulate poorly water-soluble molecules. 2-[2-[2-Chloro-3-[(1,3-dihydro-3,3-dimethyl-1-propyl-2H-indol-2-ylidene)ethylidene]-1-cyclohexen-1-yl]ethenyl]-3,3-dimethyl-1-propylindolium iodide (IR780) was chosen due to its versatile nature as a NIR light-responsive compound (photothermal agent, photosensitizer and NIR imaging dye). IR780-loaded TPGS-TOS micelles (IR780-TTM) with suitable sizes were obtained by using specific TPGS and TOS weight feed ratios during micelles formulation and these were able to encapsulate IR780 with high efficiency. In *in vitro* assays, the IR780-TTM induced a cytotoxic effect in cancer cells upon exposure to NIR irradiation through the generation of reactive oxygen species (PDT). This effective ablation of cancer cells

was achieved using an ultra-low IR780 concentration. Moreover, IR780-TTM also demonstrated the ability to act as photothermal and imaging agents.

Overall, the novel micellar nanoplatforms developed in this study possess a huge potential for breast cancer PDT. Moreover, IR780-TTM also demonstrate promising results to act as photothermal and imaging agents, which widens their applicability for the treatment and diagnosis of cancer.

Keywords

Breast cancer, IR780, photodynamic therapy, photothermal therapy, TPGS-TOS micelles.

List of Publications

Articles submitted for publication in international peer reviewed journals:

Pais-Silva, C., de Melo-Diogo, D., and Correia, I. J. *IR780-loaded TPGS-TOS micelles for breast cancer photodynamic therapy*. European Journal of Pharmaceutics and Biopharmaceutics (3.975), under review.

de Melo-Diogo, D., Pais-Silva, C., Costa, E. C., Louro, R. O., and Correia, I. J. *TPGS functionalized nanographene oxide for cancer phototherapy*. Carbon (6.198), submitted.

Poster communications:

Pais-Silva, C., de Melo-Diogo, D., and Correia, I. J. *Vitamin E-based micelles for cancer cell imaging*, V Encontro Nacional de Estudantes de Materiais (ENEM), 29th of September, Universidade da Beira Interior, Covilhã, Portugal.

Index

Figures Index

Tables Index

List of Abbreviations

ADR	adriamycin-resistant
ANOVA	analysis of variance
Bcl-2	B-cell lymphoma 2
BxPC-3	human primary pancreatic adenocarcinoma cell line
CD4 T	cluster of differentiation 4-positive lymphocyte
CLSM	confocal laser scanning microscopy
CT-26	murine colon adenocarcinoma cell line
CTL	cytotoxic T lymphocyte
DMEM-F12	Dulbecco's modified Eagle's medium F-12
DNA	deoxyribonucleic acid
Dox	doxorubicin
ECM	extracellular matrix
EE	encapsulation efficiency
EPR	enhanced permeability and retention
FBS	fetal bovine serum
FDA	food and drug administration
H_2DCF-DA	2',7'-dichlorofluorescein diacetate
Hb	deoxyhemoglobin
HbO_2	oxyhemoglobin
HCT-116	human colon carcinoma cell line
HepG2	human hepatocyte carcinoma cell line
HF	heparin-folic acid
HSA	human serum albumin
IARC	international agency for research on cancer
IC50	half maximal inhibitory concentration
ICG	indocyanine green
IFP	interstitial fluid pressure
IR780	2-[2-[2-Chloro-3-[(1,3-dihydro-3,3-dimethyl-1-propyl-2H-indol-2-ylidene)ethylidene]-1-cyclohexen-1-yl]ethenyl]-3,3-dimethyl-1-propylindolium iodide
IR780-TTM	IR780-loaded TPGS-TOS micelles
LC	loading content
MCF-7	Michigan cancer foundation-7 cell line
MDSC	myeloid-derived suppressor cell
MetOH	methanol
mPEG	methoxy poly(ethylene glycol)
MSC	mesenchymal stem cell
NIR	near-infrared

NK/T	natural killer lymphocyte/natural killer T lymphocyte
NP	nanoparticle
PBMA	poly(*n*-butylmethacrylate)
PBS	phosphate buffered saline
PCL	poly(caprolactone)
PDI	polydispersity index
PDT	photodynamic therapy
PEG	poly(ethylene glycol)
PLGA	poly(lactic-co-glycolic acid)
PMDPC	poly(12-methacryloyloxy dodecyl phosphorylcholine)
PMPC	poly(2-methacryloyloxyethyl phosphorylcholine)
PTT	photothermal therapy
RES	reticuloendothelial system
ROS	reactive oxygen species
RT	room temperature
SD	standard deviation
TEM	transmission electron microscopy
Tf	transferrin
Th2	helper type 2 lymphocyte
TME	tumor microenvironment
TOS	D-α-tocopheryl succinate
TPGS	D-α-tocopheryl polyethylene glycol 1000 succinate
Treg	regulatory T lymphocyte
TTM	TPGS-TOS micelles
UV-vis-NIR	ultraviolet-visible-near-infrared
VEGF	vascular endothelial growth factor
αSMA	alpha smooth muscle actin

Chapter 1
Introduction

1. Introduction

1.1. Cancer

1.1.1. Cancer: an evolutionary pathology with specific hallmarks

Cancer is a challenging global health problem with a growing incidence that has high morbidity and mortality rates associated (Fitzmaurice *et al.*, 2015). The International Agency for Research on Cancer (IARC) of World Health Organization estimates that there were more than eight million of cancer-related deaths worldwide in 2012 (Ferlay *et al.*, 2015). In 2016, more than one and a half million of new cases are expected to be diagnosed just in the United States of America and almost six hundred thousand cancer-related deaths will occur within the same period (Siegel *et al.*, 2016). In Portugal, the *Direção-Geral da Saúde* predicts that in 2035 more than sixty thousand people will be diagnosed with this disease (Miranda *et al.*, 2015).

Cancer is triggered by an uncontrolled proliferation process – termed carcinogenesis - where healthy cells go through profound genetic and epigenetic transformations that lead to the formation of malignant cells (Gillies *et al.*, 2012). The causes for the development of this malignant phenotype are essentially related to: (i) genetic susceptibility, (ii) environmental factors (radiation, pollution and infections), and (iii) lifestyle factors (diet, physical inactivity, tobacco and alcohol consumption) (Gillies *et al.*, 2012; Vineis and Wild, 2014). Nowadays, cancer is viewed as a complex and heterogeneous tissue formed by a mass of cancer cells in continuous proliferation that are in a dynamic interplay with surrounding/recruited stromal cells and non-cellular elements that constitute the tumor microenvironment (TME) (**Figure 1**) (Hanahan and Weinberg, 2000).

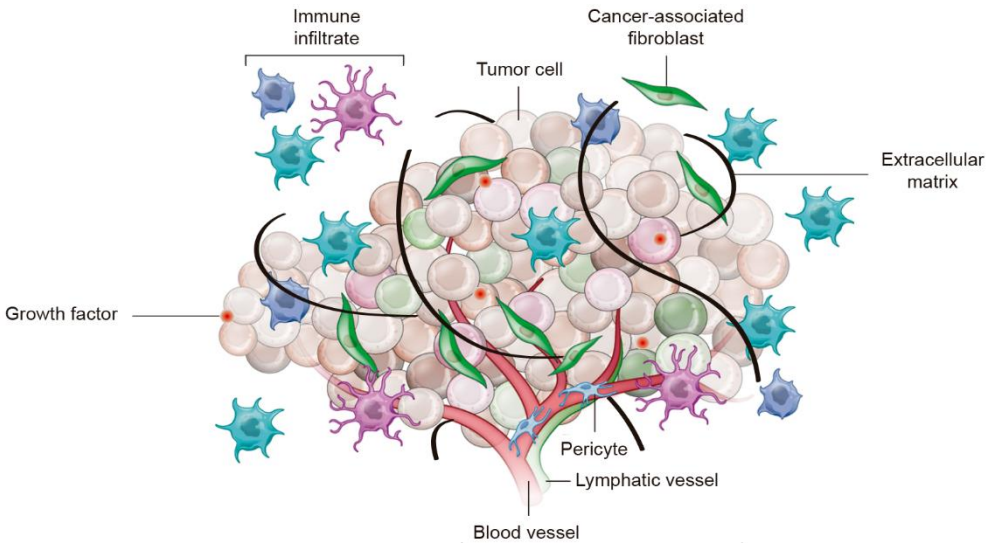

Figure 1. Representation of the cellular and non-cellular components found in tumor microenvironment and that have an active role in the process of carcinogenesis. The pro-survival, proliferation and invasion pathways of cancer cells are supported by the cross-talk between the malignant cells and the stromal cells, extracellular matrix and various signaling molecules (Adapted from (Junttila and de Sauvage, 2013)).

The tumor-associated stroma that populates the TME encompasses endothelial cells, pericytes, immune inflammatory cells and cancer-associated fibroblasts (Barcellos-Hoff *et al.*, 2013; Hanahan and Coussens, 2012), whose particular functions are summarized in **Figure 2**.

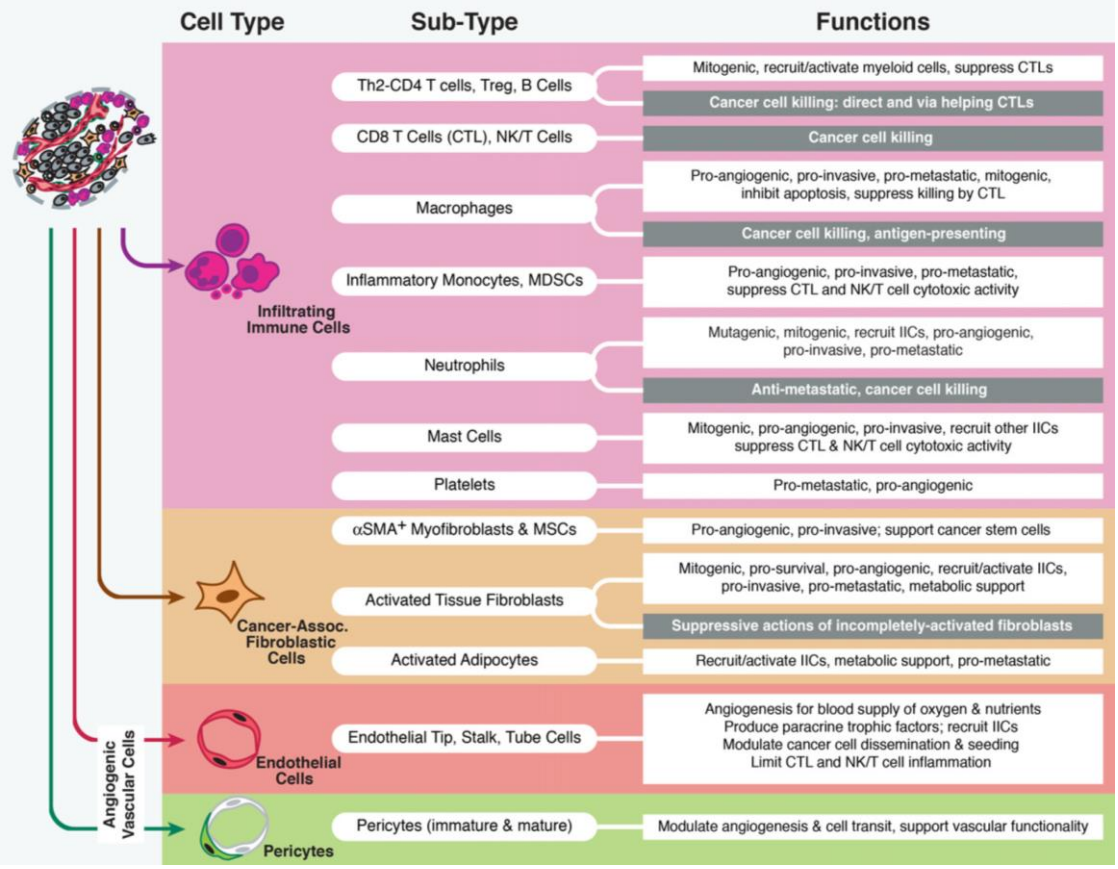

Figure 2. Description of the major types and sub-types of stromal cells that populate the tumor microenvironment and particular functions that contribute to the development and regulation of the carcinogenic process. Helper type 2 lymphocyte (Th2), cluster of differentiation 4-positive lymphocyte (CD4 T), regulatory T lymphocyte (Treg), cytotoxic T lymphocyte (CTL), natural killer lymphocyte/natural killer T lymphocyte (NK/T), myeloid-derived suppressor cell (MDSC), alpha smooth muscle actin (αSMA), mesenchymal stem cell (MSC) (Adapted from (Hanahan and Coussens, 2012)).

Apart from the cellular components, extracellular matrix (ECM), various signaling molecules and soluble mediators are also found in the TME (Pickup *et al.*, 2014; Witsch *et al.*, 2010; Xu *et al.*, 2014). The synergistic interaction between the TME elements contribute to the development and the maintenance of unique features displayed by cancer cells that Hanahan and Weinberg termed as "hallmarks of cancer" (Hanahan and Weinberg, 2000). Cancer hallmarks include the capacity to: (i) sustain proliferative signaling, (ii) evade growth suppressors, (iii) avoid programmed cell death, (iv) enable replicative immortality, (v) induce angiogenesis, and (vi) activate invasion and metastasis (**Figure 3**).

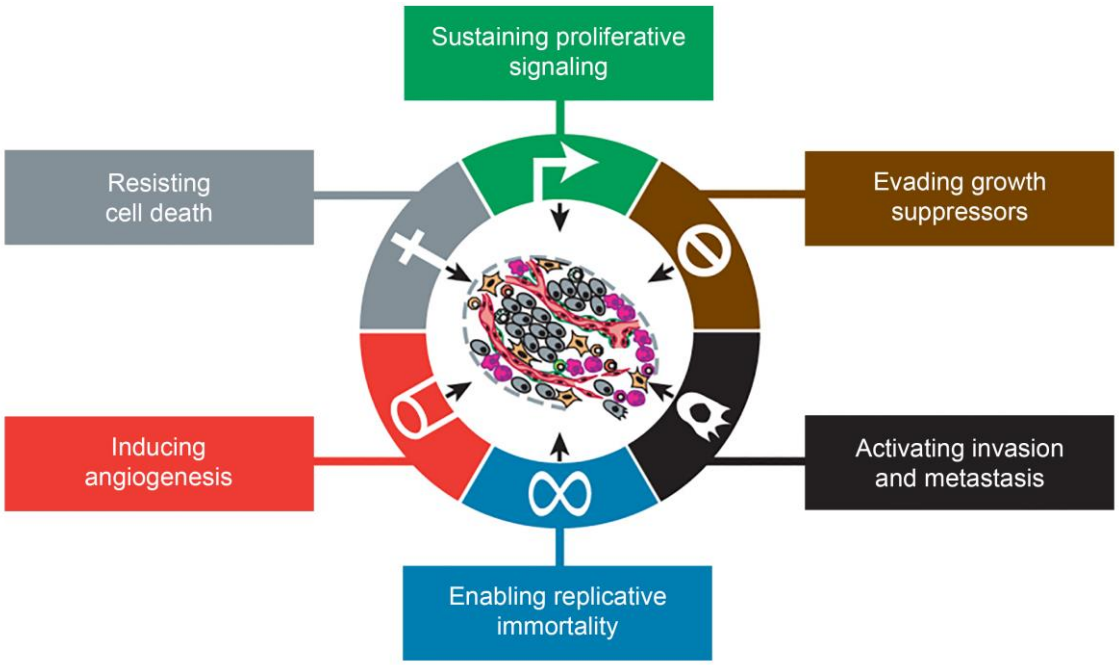

Figure 3. Hallmarks displayed by cancer cells. These hallmarks are responsible for the development and maintenance of their malignant characteristics (Adapted from (Hanahan and Weinberg, 2011)).

Cancer cells are able to proliferate by deregulating growth signaling pathways. In this process, cells can acquire autonomy in the synthesis of their own mitogenic growth factors (e.g. platelet-derived growth factor) or overexpress receptors (such as those containing intracellular tyrosine kinase domains) that are involved in growth signaling pathways (Hanahan and Weinberg, 2000; Pietras and Östman, 2010). The continuous proliferation of cancer cells is also prompted by their capacity to evade growth suppressors, like tumor suppressor protein 53 and retinoblastoma protein (Di Fiore *et al.*, 2013; Giampazolias and Tait, 2015). Moreover, cancer cells can also resist to death mechanisms by favoring the expression of anti-apoptotic proteins (like those from the B-cell lymphoma 2 (Bcl-2) family) and by circumventing pro-apoptotic signals commonly present in healthy cells (Caino *et al.*, 2009; Giampazolias and Tait, 2015; Kelly and Strasser, 2011). Furthermore, these cells also acquire replicative immortality through the overexpression of telomerase, an enzyme that adds repeated segments of hexanucleotides to the ends of telomeric deoxyribonucleic acid (DNA). The expression of high levels of telomerase by cancer cells renders them the capacity to surpass senescence, by preventing DNA damage and cell death associated with end-to-end chromosomal fusion (Caino *et al.*, 2009; Hanahan and Weinberg, 2000).

Additionally, cancer cells induce angiogenesis and metastasis, in order to have access to nutrients, oxygen and also to remove metabolic waste and carbon dioxide generated by their metabolism. The angiogenic capacity of cancer cells is induced by the switch of the quiescent state of vasculature to a permanently activated state during tumor progression, resulting from an increased expression of angiogenic inducers (e.g. vascular endothelial growth factor (VEGF) and fibroblast growth factor) (Saharinen *et al.*, 2011; Turner and Grose, 2010). Furthermore,

cancer cells may attain certain features that allow them to extravasate, invade and colonize other tissues throughout the body, resulting in the formation of metastasis (Hanahan and Weinberg, 2000). The complex and rich vascular network generated during the tumor-associated angiogenesis supports cancer cells metastization (Hanahan and Coussens, 2012). Along with this, variations in the shape and tethering of cancer cells (specifically the lack of expression of cell-cell adhesion molecules or integrins) also contribute to the mestastization process (Canel *et al.*, 2013; Chaffer and Weinberg, 2011; Hanahan and Weinberg, 2011; Yilmaz and Christofori, 2009).

More recently, owing to the remarkable progress in the field of cancer research, Hanahan and Weinberg added two additional hallmarks to the ones previously described: the ability of cancer cells to reprogram their metabolism, namely through adjustments in the glycolytic pathways, and their capacity to evade the immune system (Hanahan and Weinberg, 2011).

1.1.2. Breast cancer

Breast cancer is the most frequently diagnosed type of cancer among women (**Figure 4**). It is expected that around 249 thousand new cases will occur in 2016 in the United States of America, accounting for 29 % of all female cancer cases (Siegel *et al.*, 2016). Furthermore, according to the latest IARC report, in 2012 more than half a million women died from breast cancer, placing it as the leading cause of female cancer-related deaths worldwide (Torre *et al.*, 2016).

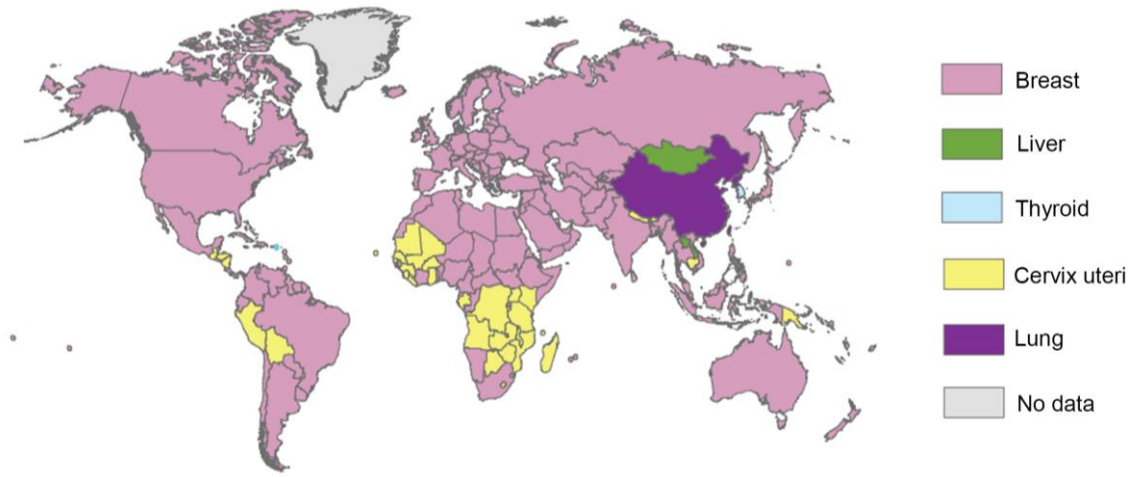

Figure 4. Most commonly diagnosed types of cancer in women worldwide in 2012, according to the estimates of the International Agency for Research on Cancer (Adapted from (Torre *et al.*, 2016)).

Breast cancer is intimately associated with gender, since females have a higher propensity for its development (Colditz *et al.*, 2014; Trichopoulos *et al.*, 2008). Moreover, the risk of developing this disease also increases with aging and it is influenced by the family history, inherited mutations (e.g. in breast cancer susceptibility genes 1 and 2), and reproductive factors (Rudolph *et al.*, 2016; Singletary, 2003; Trichopoulos *et al.*, 2008). Furthermore, environmental (e.g. exposure to radiation) and lifestyle factors (e.g. obesity, diet or physical

inactivity) can also influence the emergence of this disease (Colditz *et al.*, 2014; Singletary, 2003; Trichopoulos *et al.*, 2008).

Breast cancer carcinogenesis comprises several stages that are governed by genetic and epigenetic alterations (**Figure 5**) (Polyak, 2007). In normal breast ducts, a layer of luminal epithelial and myoepithelial cells is found in the basement membrane, which is surrounded by the cells that compose the stroma (fibroblasts, myofibroblasts, leukocytes and endothelial cells) (Polyak, 2007). When myoepithelial cells decrease in number (presumably due to degradation of the basement membrane) and undergo through epigenetic and phenotypic alterations, together with an increment of the stromal cells, an *in situ* carcinoma is developed (Polyak, 2007). The subsequent total loss of myoepithelial cells and basement membrane results in the establishment of an invasive carcinoma (Polyak, 2007). Ultimately, tumor cells may invade the surrounding tissues and colonize distant sites in the body, leading to the appearance of breast cancer metastasis (Polyak, 2007).

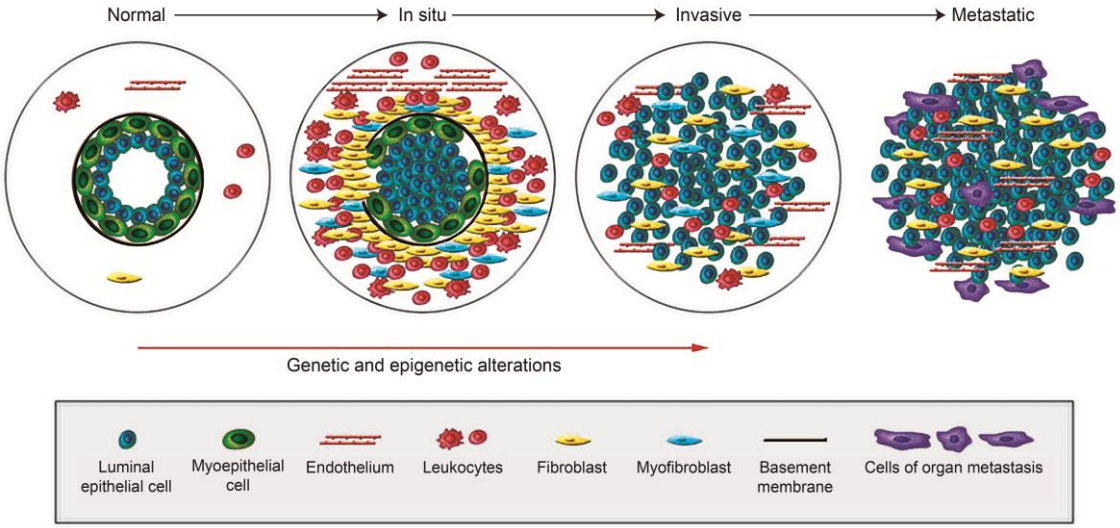

Figure 5. Schematic representation of the breast cancer carcinogenesis. Breast cancer emerges as a consequence of genetic and epigenetic alterations that occur in myoepithelial cells, together with a reduction in their number. At the same time, the basement membrane starts to degrade and the population of stromal cells (lymphocytes, fibroblasts, myofibroblasts and endothelial cells) increases, resulting in the formation of an *in situ* carcinoma. The subsequent total loss of myoepithelial cells and basement membrane results in the development of invasive carcinomas, which can spread to distant sites of the body, leading to the formation of breast cancer metastasis (Adapted from (Polyak, 2007)).

Breast cancer can have a different answer to treatments due to its heterogeneity, which is characterized by several clinical, morphological and molecular features (Polyak, 2011; Zardavas *et al.*, 2015). Currently, the standard treatment options for breast cancer include surgery, radiation therapy and small molecule-based therapies (chemo, hormone or targeted therapies) (DeSantis *et al.*, 2014). When cancer is diagnosed at an early stage, the surgical resection of the tumor is usually performed to remove the majority of the tumor mass (Wyld *et al.*, 2015). This treatment may also be complemented with radiotherapy and/or small molecule-based therapies (Wyld *et al.*, 2015). Late-stage breast cancer is treated with small molecule-based

therapies due to the existence of metastasis throughout the body (Tryfonidis *et al.*, 2015; Twelves *et al.*, 2016).

However, the currently available therapies are not selective since they damage both cancer and healthy cells, leading to the occurrence of adverse side effects that may span from fatigue, nausea or hair loss to organ failure (Runowicz *et al.*, 2016). Moreover, cancer cells often develop resistance mechanisms to radio and small molecule-based therapies, which further decreases the effectiveness of the available treatments (Blanco and Ferrari, 2014; Tang *et al.*, 2016). Due to these drawbacks, researchers and clinicians are currently investigating new therapeutic approaches to increase the efficacy and safety of breast cancer treatments.

1.1.3. Phototherapies

Within the panoply of cancer therapies under investigation, light-induced treatments have been demonstrating promising results (Huggett *et al.*, 2014; Lucky *et al.*, 2015). After the administration of light-responsive molecules, the tumor zone is irradiated with light and thus the compounds accumulated within this area will produce the desired therapeutic effect (Cheng *et al.*, 2014). The compounds that may have accumulated in other sites will not produce any cytotoxic effects since those areas are not exposed to light. Exceptionally, compounds accumulated within organs that are in the light path (e.g. skin) can induce some degree of toxicity. Therefore, this therapeutic modality offers some tumor selectivity when compared to conventional therapies (Cheng *et al.*, 2014).

The most promising phototherapeutic agents under investigation are those that strongly absorb in the near-infrared (NIR) region (750 – 1000 nm) due to their capacity to interact with NIR light. NIR radiation is within the so-called biological transparency window, meaning that its interaction with biological components (e.g. hemoglobin, myoglobin, melanin or water) is minimal (**Figure 6**) (Cheng *et al.*, 2014; Rwei *et al.*, 2015; Thakor and Gambhir, 2013). Moreover, NIR light also ensures deep tissue penetration, which is fundamental for the radiation to reach the photoabsorbers accumulated in the tumor zone.

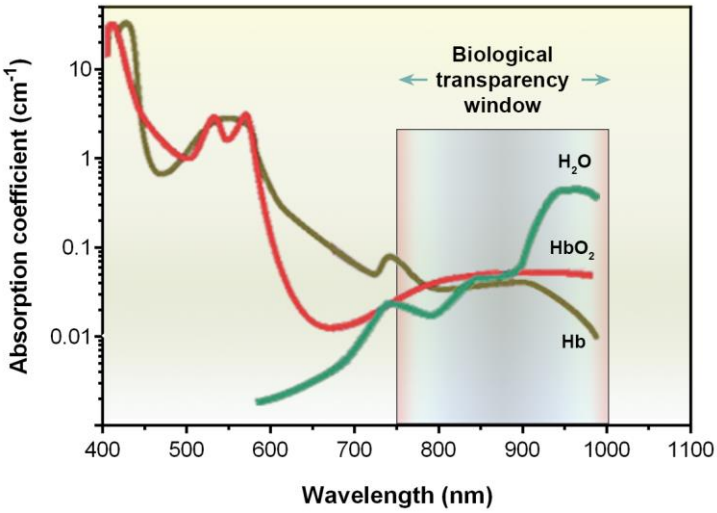

Figure 6. Representation of the biological transparency window (750 – 1000 nm) and the ultraviolet-visible-near-infrared (UV-vis-NIR) absorption spectra of the main biological components of the human tissues. Within 750 - 1000 nm the biological components display a minimal absorbance, conferring NIR light deep tissue penetration and low off-target interactions. Oxyhemoglobin (HbO_2), deoxyhemoglobin (Hb) (Adapted from (Rwei *et al.*, 2015)).

There are two classes of NIR photoabsorbers: the photosensitizers that are used in photodynamic therapy (PDT) and the photothermal agents that are employed in photothermal therapy (PTT) (Cheng *et al.*, 2014). In PDT, the administrated photosensitizers are activated after their exposition to light, that leads to an energy transfer between the photosensitizers and the molecular oxygen that culminates in the generation of reactive oxygen species (ROS). ROS cause tumor ablation through three main mechanisms: (i) by killing the tumor cells, (ii) damaging the normal and the tumor-associated vasculature, and (iii) activating inflammatory and immune responses against tumor cells (Dolmans *et al.*, 2003; Lucky *et al.*, 2015; Tong and Kohane, 2012). The extent of the PDT-induced cytotoxicity is affected by the optical properties and the concentration of the photosensitizers used and by its localization (intra- or extracellular space), the time span between the photosensitizers administration and the light exposure, and the oxygen availability in the tumor area (Dolmans *et al.*, 2003; Lucky *et al.*, 2015). Photofrin® is a Food and Drug Administration (FDA)-approved photosensitizer used for cancer PDT (Lucky *et al.*, 2015; Tong and Kohane, 2012). However, this photosensitizer is usually irradiated with 630 nm light, due to its intrinsic properties, which reduces the penetration depth attained by this therapy. Moreover, Photofrin® also displays a low molar extinction coefficient, which demands the administration of high concentrations of this molecule and the application of intense irradiation to achieve the desired therapeutic effect (Dolmans *et al.*, 2003; Lucky *et al.*, 2015).

Similarly, PTT starts with the administration of photothermal agents to the patient, followed by the irradiation of the tumor zone. However, the mechanism of action of PTT relies on the thermal ablation of cancer cells, through the ability of the photothermal agents to convert the absorbed light into heat (Cheng *et al.*, 2014; Tong and Kohane, 2012). If temperature increases to above 50 °C, cell death through coagulation necrosis process can occur. When lower

temperatures (41-45 °C) are reached, cellular functions can be compromised (e.g. DNA repair or mitochondrial activity), resulting in damage to cancer cells (Chu and Dupuy, 2014). Moreover, this hyperthermic effect can also sensitize cancer cells to radio and chemotherapies (Jaque *et al.*, 2014). In this way, the optical properties and photothermal conversion efficiency of the photothermal agents are crucial for the therapeutic outcome (Song *et al.*, 2015). Furthermore, the availability of the photothermal agents within the TME, their cellular distribution and the onset of the irradiation also affect therapeutic effectiveness (Tong and Kohane, 2012). NIR dye indocyanine green (ICG) is approved by FDA for clinical applications and has been widely investigated for cancer PTT. Nevertheless, the poor stability of ICG in aqueous media and concentration-dependent aggregation limit its applications in medicine (Cheng *et al.*, 2014; Song *et al.*, 2015).

More recently, 2-[2-[2-Chloro-3-[(1,3-dihydro-3,3-dimethyl-1-propyl-2H-indol-2-ylidene) ethylidene]-1-cyclohexen-1-yl]ethenyl]-3,3-dimethyl-1-propylindolium iodide (IR780), a hydrophobic heptamethine indocyanine dye, started to be explored as a light-responsive agent for cancer therapy (Peng *et al.*, 2011; Wang *et al.*, 2016). The characteristic absorption peak of IR780, at 780 nm, enables its effective interaction with NIR light (Han *et al.*, 2015). Additionally, IR780 presents a good quantum yield and reduced photobleaching (Zhang *et al.*, 2010). In fact, as a NIR dye, IR780 presents a higher molar extinction coefficient than Photofrin® and it is also able to reach deeper diseased tissues (Bazylińska *et al.*, 2014; Dolmans *et al.*, 2003). Moreover, comparatively to ICG, IR780 has higher photostability and fluorescence intensity, endowing IR780-based therapies an even higher potential for cancer phototherapy (Yuan *et al.*, 2015). Currently, IR780 has been reported to produce ROS, temperature increase or both effects upon NIR irradiation, that along with its good NIR fluorescence enables its use as a phototherapeutic (PDT and PTT) and imaging agent (Peng *et al.*, 2011; Wilk *et al.*, 2012; Zhang *et al.*, 2010). However, the clinical application of this versatile photoresponsive molecule is strongly impaired by its low solubility in pharmaceutically acceptable solvents (Jiang *et al.*, 2015). To surpass such handicap, IR780 encapsulation in nanoparticles (NPs) has been proposed for improving its therapeutic efficacy.

1.2. Nanomaterials for application in cancer phototherapy

1.2.1. The potential of unifying the best of both worlds

For improving the effectiveness and selectivity of PDT and PTT towards cancer cells, researchers have been encapsulating NIR light-responsive molecules in NPs (**Figure 7**) (Dolmans *et al.*, 2003; Tong and Kohane, 2012; Wust *et al.*, 2002).

NPs can be composed by organic or inorganic materials and display a size that spans from 1 to 1000 nm (Ferrari, 2005; Jain and Stylianopoulos, 2010; Petros and DeSimone, 2010; Schroeder *et al.*, 2012). These nanostructures can be used to encapsulate NIR photosensitizer and photothermal agents, which is fundamental to overcome their low water solubility, degradation and photobleaching issues (Lucky *et al.*, 2015; Thakor and Gambhir, 2013; Tong and Kohane, 2012). Moreover, NPs can also display a preferential accumulation in tumors, which in turn improves the availability of the loaded NIR photoabsorbers at the tumor zone. Thereby, this approach also reduces the non-specific toxicity of phototherapies towards healthy cells/tissues and decreases the light exposure (duration and intensity) required to achieve a suitable therapeutic effect (Farokhzad and Langer, 2009; Lucky *et al.*, 2015; Rwei *et al.*, 2015; Thakor and Gambhir, 2013; Tong and Kohane, 2012).

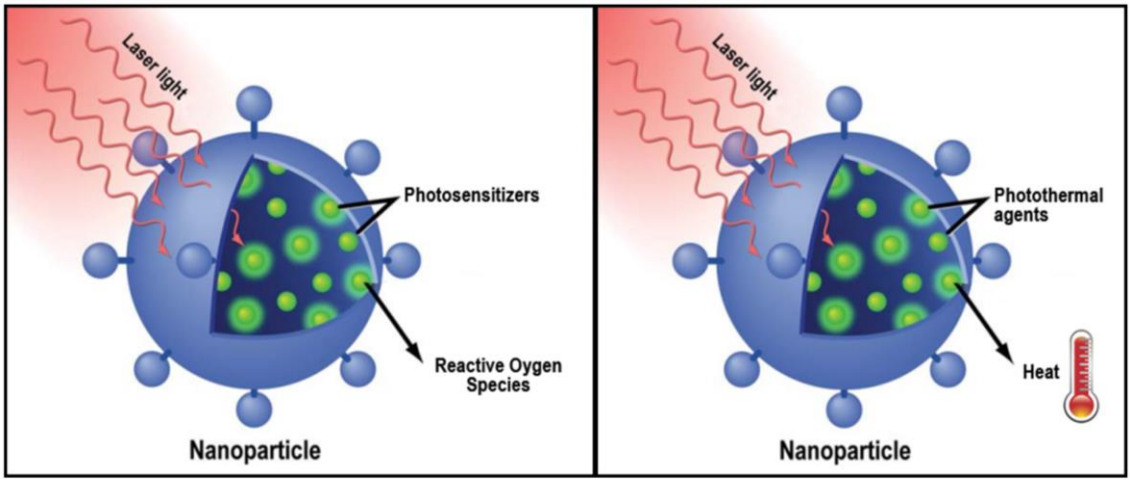

Figure 7. Representation of the mechanism of action of nanoparticles-mediated photodynamic therapy (left) and photothermal therapy (right). In this type of therapeutic approach, nanoparticles are used to load photoabsorbers and deliver them to tumor cells. Within the cells, the entrapped photoabsorbers are stimulated by near-infrared light to generate reactive oxygen species (photodynamic therapy) or heat (photothermal therapy) that induce cellular damage (Adapted from (Thakor and Gambhir, 2013)).

For a successful NP-mediated phototherapy, these nanosized agents must be carefully designed in order for them to display a specific size, morphology, charge and corona composition. These parameters influence the pharmacokinetic profile of the NPs and will, ultimately, determine the dose of photosensitizers/photothermal agents delivered into the tumor by the NPs and thus the therapeutic outcome (Ernsting *et al.*, 2013; Kaur *et al.*, 2016; Lucky *et al.*, 2015).

1.2.2. NPs-mediated phototherapy: the design drives the journey

NPs loading NIR photoabsorbers can be administered by intratumoral or intravenous injections (Etheridge *et al.*, 2013; Petros and DeSimone, 2010). Since the majority of the FDA-approved NPs for cancer therapy are administered intravenously, this section will be focused on the presentation of the design requirements that NPs loaded with NIR photoabsorbers should fulfill considering this administration route (**Figure 8**) (Ernsting *et al.*, 2013; Ferrari, 2005).

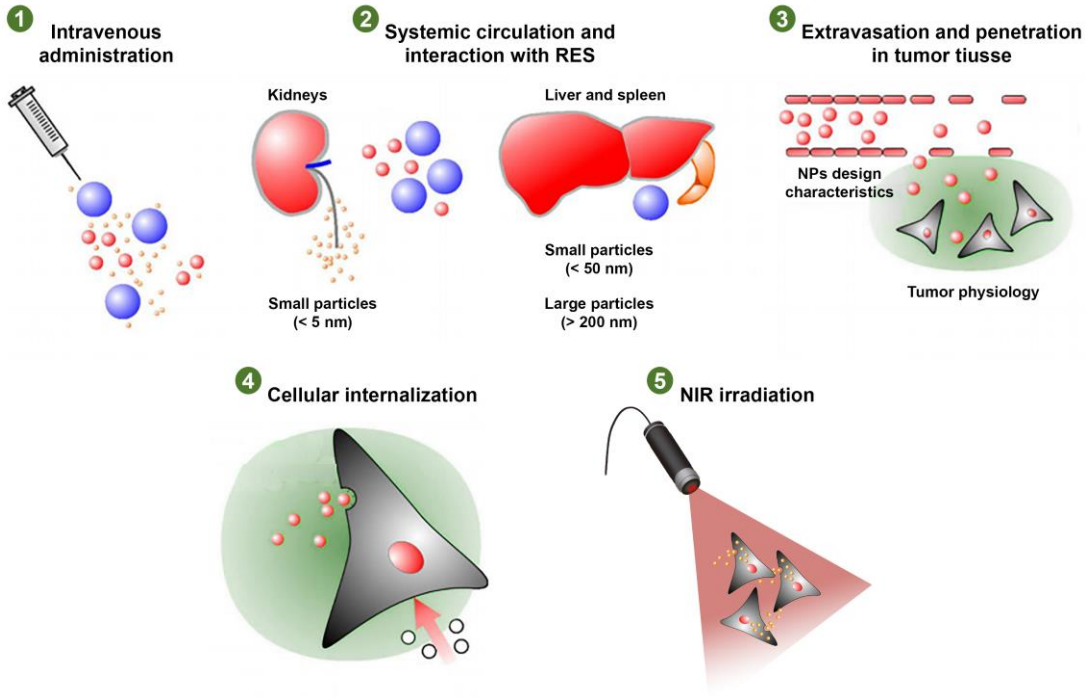

Figure 8. Illustration of the different stages of nanoparticles-mediated phototherapy. Factors that influence nanoparticles blood circulation (e.g. size), extravasation from the blood flow to the tumor zone (e.g. nanoparticles features) and penetration in the tumor mass (nanoparticles features and tumor-related factors) are represented. Reticuloendothelial system (RES), near-infrared (NIR) (Adapted from (Luo *et al.*, 2015)).

Once intravenously injected, NPs must sustain their structural integrity and protect the loaded photoabsorbers (**Figure 8**). Such is fundamental to avoid the leakage of the loaded compounds, which in turn could lead to its degradation and clearance from blood circulation or even result in undesirable pharmacokinetics (accumulation in off-target organs) (Blanco *et al.*, 2015; Ernsting *et al.*, 2013). NPs must be able to avoid renal filtration and opsonization by blood proteins (serum albumin, complement components, apolipoproteins and immunoglobulins). These opsonins adsorb on the surface of NPs enabling their recognition and phagocytosis by the reticuloendothelial system (RES) cells (Aggarwal *et al.*, 2009; Blanco *et al.*, 2015). NPs size, charge and corona composition have a key role in this phase of the phototherapeutic procedure (Ernsting *et al.*, 2013).

NPs must not be smaller than 5 nm or otherwise they will be removed from circulation through renal filtration (Blanco *et al.*, 2015). Moreover, nanostructures with a size lower than 50 nm tend to become accumulated in the liver since these can extravasate through the liver

fenestrations, which have a size that is comprehended between 50-100 nm (Blanco *et al.*, 2015; Ernsting *et al.*, 2013). On the other hand, the splenic filtration governs the upper size limit. Splenic interendothelial slits present a size range from 200 to 500 nm and impose 200 nm as the maximal NP size that is able to evade retention in the spleen (Blanco *et al.*, 2015; Petros and DeSimone, 2010). Furthermore, NPs with a size higher than 200 nm are also more likely to be phagocytized by liver Kupffer cells and by splenic macrophages (Blanco *et al.*, 2015; Ernsting *et al.*, 2013; Luo *et al.*, 2015).

NPs surface charge also determines their biological fate during blood circulation. Generally, negatively charged (zeta potential < 10 mV) nanocarriers tend to have a high uptake by RES macrophages, while those with a positive surface charge (zeta potential > 10 mV) display a high propensity for protein adsorption on their surface (Ernsting *et al.*, 2013). Hence, NPs should have a superficial charge of ± 10 mV, the so-called neutral charge range, in order to exhibit low protein adsorption and low accumulation in RES organs (Blanco *et al.*, 2015; Ernsting *et al.*, 2013; Stylianopoulos and Jain, 2015).

The surface composition of NPs is another important parameter that mediates their interaction with serum proteins and RES components. To avoid such undesirable interactions, the surface of NPs is commonly modified with poly(ethylene glycol) (PEG). This type of functionalization stabilizes the NPs and also prevents their opsonization and phagocytosis by RES cells (Blanco *et al.*, 2015; Ernsting *et al.*, 2013; Jain and Stylianopoulos, 2010; Stylianopoulos and Jain, 2015). Still, the benefits of PEGylation are not always attained since these depend on of multiple factors such as the molecular weight and density of the PEG chains (Aggarwal *et al.*, 2009; Ernsting *et al.*, 2013). Currently, other polymers are also being investigated as alternatives to PEG, such as poly(aminoacid)s (e.g. poly(glutamic acid)) and poly(oxazolines) (Barz *et al.*, 2011; Knop *et al.*, 2010).

Besides avoiding its clearance by kidneys and RES, NPs must be able to extravasate from the blood flow to the tumor site (**Figure 8**). Tumor vasculature presents fenestrations that vary from 400 to 600 nm, which are permeable to NPs. In this way, NPs may benefit from this leaky vasculature to extravasate into the tumor interstitial space (Danhier *et al.*, 2010; Ernsting *et al.*, 2013). Moreover, the impaired lymphatic drainage present in this tissue promotes NPs retention in the TME (Bertrand *et al.*, 2014; Danhier *et al.*, 2010). This phenomenon is known as the Enhanced Permeability and Retention (EPR) effect (Bertrand *et al.*, 2014; Danhier *et al.*, 2010; Ernsting *et al.*, 2013). Taking these and the previous size impositions into consideration, NPs should have a size of 100-200 nm in order to be minimally cleared by off-target organs and display an enhanced tumor accumulation through the EPR effect (Blanco *et al.*, 2015; Petros and DeSimone, 2010).

Once in the tumor interstitial space, NPs must penetrate through the tumor biomass in order to reach the cancer cells (**Figure 8**). Their efficient penetration depends on factors intrinsic to

the tumor physiology and NPs features (Ernsting *et al.*, 2013). Tumor physiological factors comprise tumor vasculature, interstitial fluid pressure (IFP) and the presence of cells that populate the TME (Danhier *et al.*, 2010; Ernsting *et al.*, 2013).

As a consequence of the aberrant and heterogeneous tumor vasculature, the tumor periphery is highly perfused whereas its core is hypoxic (Blanco *et al.*, 2015; Ernsting *et al.*, 2013). In this way, most of the NPs become accumulated in tumor periphery leading to a heterogeneous NP distribution (Ernsting *et al.*, 2013). Moreover, the tumor vasculature and the impaired lymphatic drainage are responsible for the presence of a high IFP in the tumor, which also hinders the penetration of NPs through the tumor biomass (Blanco *et al.*, 2015; Jain and Stylianopoulos, 2010). Furthermore, the cells that populate the TME can also hamper NPs penetration (Blanco *et al.*, 2015; Ernsting *et al.*, 2013; Jain and Stylianopoulos, 2010).

On the other hand, NPs-related characteristics such as their size and charge also determine their penetration through the tumor tissue (Ernsting *et al.*, 2013). Generally, smaller NPs have a better tumor penetration capacity than those with larger dimensions (Bertrand *et al.*, 2014; Ernsting *et al.*, 2013; Jain and Stylianopoulos, 2010; Stylianopoulos and Jain, 2015). Moreover, positively charged NPs have a higher propensity to interact with the hyaluronic acid present in tumor ECM than those with a negative charge, that are more prone to interact with collagen (Ernsting *et al.*, 2013; Jain and Stylianopoulos, 2010). In this way, neutral charged NPs display a better penetration capacity since they establish a lower number of interactions with tumor ECM components (Ernsting *et al.*, 2013).

Finally, the photoabsorber-loaded NPs must then be internalized by cancer cells (**Figure 8**). Such is fundamental to achieve an effective and selective therapeutic effect upon NIR laser irradiation. The main parameters affecting NPs cellular internalization are related to their size, charge and the presence of targeting ligands on their surface (Blanco *et al.*, 2015; Ernsting *et al.*, 2013).

NPs usually have an optimal size for cellular internalization, which varies for each type of NP (Hillaireau and Couvreur, 2009; Nel *et al.*, 2009; Petros and DeSimone, 2010). In terms of charge, particles with a positive surface charge are more likely to be internalized by cells, since these are able to establish interactions with the negatively charged components of cells' membrane (Stylianopoulos and Jain, 2015). However, the previous considerations about positively charged NPs should still be taken into consideration since these are more likely to adsorb proteins, which may result in their clearance during blood circulation (Bertrand *et al.*, 2014; Ernsting *et al.*, 2013). Additionally, NPs surface can be decorated with targeting ligands in order to promote their uptake by cancer cells overexpressing the receptor for the immobilized ligand (Nel *et al.*, 2009).

Therefore, the efficacy of NPs-mediated phototherapies is strongly influenced by NPs physicochemical properties and also by the properties of the photoabsorbers and external light, as previously described.

1.2.3. Nanovehicles classes: different characteristics for multiple applications

Currently, there are different types of NPs that have shown the capacity to encapsulate hydrophobic molecules, such as NIR photoabsorbers, and to deliver them to cancer cells (Cheng *et al.*, 2014; Jaque *et al.*, 2014; Kim *et al.*, 2016; Lucky *et al.*, 2015; Pekkanen *et al.*, 2014; Rwei *et al.*, 2015; Tong and Kohane, 2012). In a broad sense, these NPs can be divided into two main classes: organic and inorganic NPs (see **Figure 9** for further details) (Wicki *et al.*, 2015).

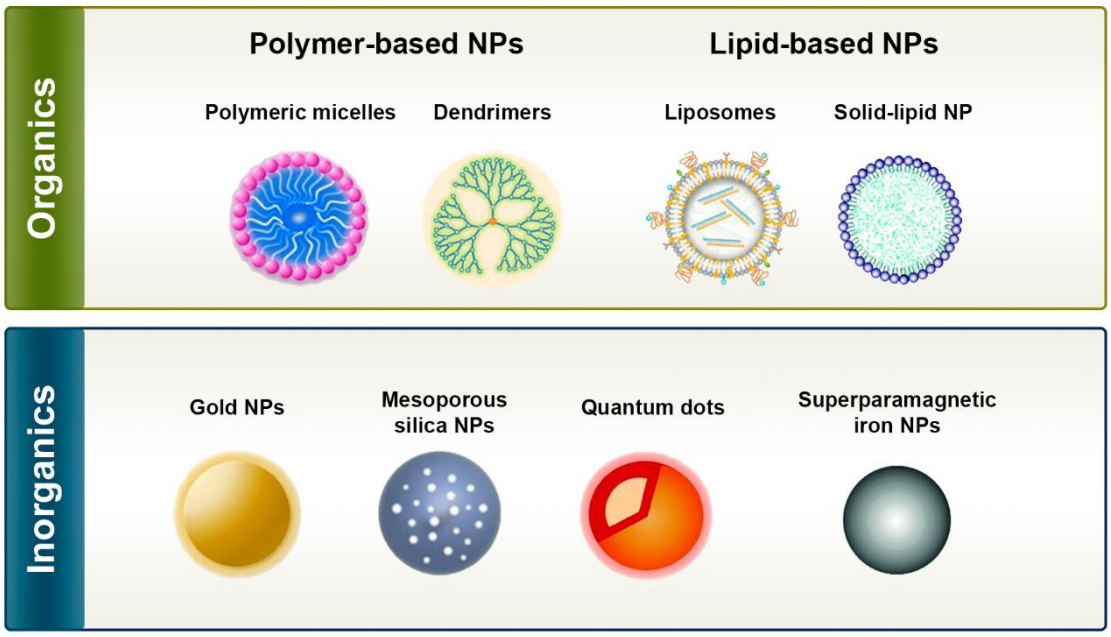

Figure 9. Examples of the different types of nanoparticles that can be used to encapsulate near-infrared photoabsorbers. These types of nanoparticles have specific characteristics that allow their application in cancer therapy and/or diagnosis (Adapted from (McCarthy *et al.*, 2015) and (Wicki *et al.*, 2015)).

Organic NPs are produced with natural or synthetic compounds and comprise polymer-based nanocarriers (micelles and dendrimers) and lipid-based nanocarriers (liposomes and solid-lipid NPs) (**Figure 9**). Polymeric micelles are formulated with amphiphilic polymers and have a core-shell organization, that comprises a hydrophobic core capable of encapsulating hydrophobic molecules and a hydrophilic shell that provides stability to the nanostructure (Nazir *et al.*, 2014). Dendrimers are hyperbranched nanostructures with a central core, that can be used to encapsulate molecules through covalent and non-covalent binding (Cheng and Xu, 2008). Liposomes are closed spherical vesicles containing an aqueous core surrounded by one or more concentric lipid bilayers that are able to entrap both hydrophobic and hydrophilic molecules (Al-Jamal and Kostarelos, 2011). Solid-lipid NPs are produced with solid lipids (at room and body temperature) that are stabilized by surfactants (Wissing *et al.*, 2004). These type of NPs

possess a rigid core that can be used to encapsulate hydrophobic and hydrophilic molecules (Thakor and Gambhir, 2013; Wissing *et al.*, 2004).

Gold NPs, quantum dots, mesoporous silica NPs and superparamagnetic iron oxides are examples of inorganic nanocarriers (**Figure 9**). Gold NPs and quantum dots are nanostructures that have been widely applied in cancer imaging and that can also be used for encapsulating therapeutic molecules (Jia *et al.*, 2013; Sun *et al.*, 2014). Mesoporous silica NPs due to their large pore volume and high superficial area have a high drug loading capacity (Rosenholm *et al.*, 2010). Superparamagnetic iron oxides can be employed as imaging and magnetic field-responsive therapeutic agents (Nazir *et al.*, 2014).

Each type of NP has specific characteristics that enable their utilization in cancer therapy. Polymeric micelles will be the focus of the next section since these are promising candidates for the delivery of NIR photoabsorbers to cancer cells.

1.2.4. Polymeric micelles

1.2.4.1. Polymeric micelles application in cancer phototherapy

Polymeric micelles display a core-shell organization resulting from the self-assembly of amphiphilic molecules in aqueous environment. In this process, the hydrophobic blocks form the core which is responsible for entrapping the hydrophobic NIR photoabsorbers. The hydrophilic segments form the corona that is responsible for the stabilization of the nanostructure (**Figure 10**) (Jones and Leroux, 1999; Kedar *et al.*, 2010; Owen *et al.*, 2012).

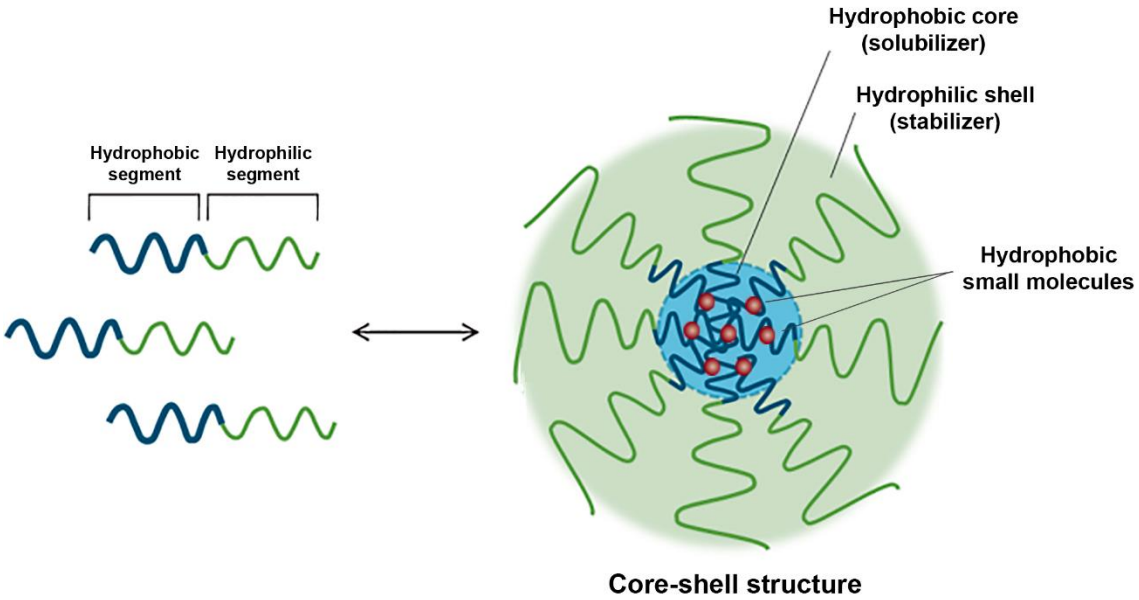

Figure 10. Representation of the polymeric micelle assembling process and of the core-shell organization (Adapted from (Owen *et al.*, 2012)).

Furthermore, the unique features presented by micelles make them very effective vehicles for the delivery of NIR photoabsorbers, such as: (i) straightforward formulation, (ii) high encapsulation efficiency (EE), (iii) great stability in circulation, (iii) suitable physicochemical characteristics to benefit from the EPR effect, (iv) biocompatibility, and (v) biodegradability (Gong *et al.*, 2012; Kedar *et al.*, 2010; Owen *et al.*, 2012).

Micelles' corona is typically composed by PEG since this hydrophilic polymer provides stealth properties to nanostructures, thereby preventing their opsonization and uptake by RES cells (Owen *et al.*, 2012). Such is fundamental to enhance micelles' blood circulation time, which in turn favors their accumulation in the tumor through the EPR effect (Knop *et al.*, 2010; Owen *et al.*, 2012). Regarding micelles' core, this can be composed of hydrophobic polymers such as poly(caprolactone) (PCL) or poly(lactic-co-glycolic acid) (PLGA), or hydrophobic blocks such as cholesterol or deoxycholic acid (Kedar *et al.*, 2010; Park *et al.*, 2004; Yu *et al.*, 2013) due to their good loading capacity. For instance, Master and co-workers prepared PEG-PCL micelles loaded with the photosensitizer silicon phtalocyanine 4, that produced a cytotoxic effect towards cancer cells under NIR laser irradiation (Master *et al.*, 2012). In another work, Zheng and co-workers synthesized micellar carriers composed of PLGA-lecithin-PEG loading the photothermal agent ICG. Their results demonstrated that these nanovehicles are efficient agents for cancer PTT (Zheng *et al.*, 2013). These observations attest the suitability of using polymeric micelles in cancer PDT and PTT.

Currently, other materials are being explored to form novel and improved micellar nanocarriers. Particularly, vitamin E derivatives arise as promising candidates to produce micelles that are able to deliver NIR photoabsorbers. Here, they were selected to produce the carriers.

1.2.4.2. Vitamin E-based micelles aimed for cancer phototherapy

Vitamin E family is constituted by eight forms of both tocopherols and tocotrienols naturally occurring as alpha (α), beta (ß), gamma (δ) and delta (γ) isomers. Vitamin E derivatives have been applied in different areas of the biomedical field (Youk *et al.*, 2005).

D-α-tocopheryl succinate (TOS) is a vitamin E derivative with anticancer properties (Duhem *et al.*, 2014b; Youk *et al.*, 2005). TOS exert its antitumoral activity through two main mechanisms: inhibition of tumor cells proliferation and induction of apoptosis. The antiproliferative activity of TOS is related to its capacity to: (i) inhibit DNA synthesis, (ii) induce cell cycle arrest, and (iii) interfere with the expression of cell cycle proteins (e.g. downregulating nuclear transcription factor-kappa B) (Constantinou *et al.*, 2008; Duhem *et al.*, 2014b). Furthermore, TOS induces apoptosis through activation of extrinsic and intrinsic apoptotic pathways (Constantinou *et al.*, 2008; Duhem *et al.*, 2014b; Youk *et al.*, 2005). The former involves the upregulation of Fas/Fas receptor and restoration of transforming growth factor pathway in cancer cells, while the latter relies on the production of ROS that leads to mitochondrial

dysfunctions (Duhem *et al.*, 2014b). In addition, TOS may also hinder angiogenesis and metastization by inhibiting VEGF and matrix metalloproteinases-9 functions, respectively (Duhem *et al.*, 2014b). However, the biomedical use of TOS is limited by its low water solubility (Duhem *et al.*, 2014b; Youk *et al.*, 2005).

D-α-tocopheryl polyethylene glycol 1000 succinate (TPGS), a PEGylated vitamin E derivative produced through the esterification of TOS with a PEG chain of 1000 Da, has also been employed in cancer therapy (Zhang *et al.*, 2012). In fact, TPGS has been described as being more potent in generating ROS, inducing apoptosis and inhibiting tumor cells growth than TOS (Youk *et al.*, 2005). Moreover, the mechanisms of TPGS-mediated apoptosis seem to result from its capacity to inhibit protein kinase B phosphorylation that is involved in the downregulation of the anti-apoptotic proteins Survivin and Bcl-2, leading to cell death through the activation of caspase-mediated apoptotic pathways. It was also verified that TPGS induces the activation of caspase-independent apoptosis and cell cycle arrest (Neophytou *et al.*, 2014). Additionally, TPGS has also demonstrated the capacity to inhibit P-glycoprotein, a drug efflux pump implied in cancer cells drug-resistance mechanisms (Collnot *et al.*, 2007).

The amphiphilic character of TPGS together with its intrinsic anticancer activity provide several advantages for its application in micelles' production (Zhang *et al.*, 2012). Moreover, TPGS-based nanomedicines have an increased cellular uptake, which also accounts for their good therapeutic potential (Kulkarni and Feng, 2013). For instance, Kutty and Feng demonstrated that Docetaxel-loaded TPGS micelles produce an anticancer therapeutic effect that is superior to that of the free drug (Kutty and Feng, 2013). However, these micelles demonstrated a size of about 18 nm, which may have a negative impact on their biodistribution. More recently, Danhier *et al.* prepared micelles using a combination of TPGS and TOS, and they were used to encapsulate doxorubicin (Dox). In TPGS-TOS micelles (TTM), the tocopherol (hydrophobic) moieties of TOS and TPGS form the core (encapsulates the hydrophobic drug), while the PEG chains (hydrophilic) of TPGS originate the shell (stabilizes the micelle). However, the Dox-loaded TTM had a size of 350 nm, which is not suitable for passive tumor accumulation and emphasizes the need to optimize the physicochemical properties of this promising delivery system (Danhier *et al.*, 2014).

TTM appear to be promising vehicles for the encapsulation and delivery of NIR photoabsorbers, since the final physicochemical properties of these micelles can be adjusted by controlling their TPGS and TOS content, and also due to the intrinsic anticancer activity of both vitamin E derivatives. Moreover, TPGS and TOS are already approved by FDA and European Medicines Agency as pharmaceutical solubilizers, which attests their biological safety (Danhier *et al.*, 2014). In this context, the encapsulation of IR780 in TTM seems to be a promising strategy for cancer phototherapy since it aims to: (i) overcome IR780 poor water solubility, (ii) take advantage of the excellent properties of micelles in cancer drug delivery, (iii) benefit from vitamin E intrinsic anticancer activities, and (iv) produce an anticancer treatment responsive

to NIR light by exploring the photoversatility of IR780 (photosensitizer, photothermal agent and imaging agent). Herein, TPGS and TOS were used to produce micelles that were exploited to encapsulate the NIR agent IR780 (IR780-TTM; **Figure 11**) and their therapeutic efficacy under NIR irradiation was evaluated using breast cancer cells as models.

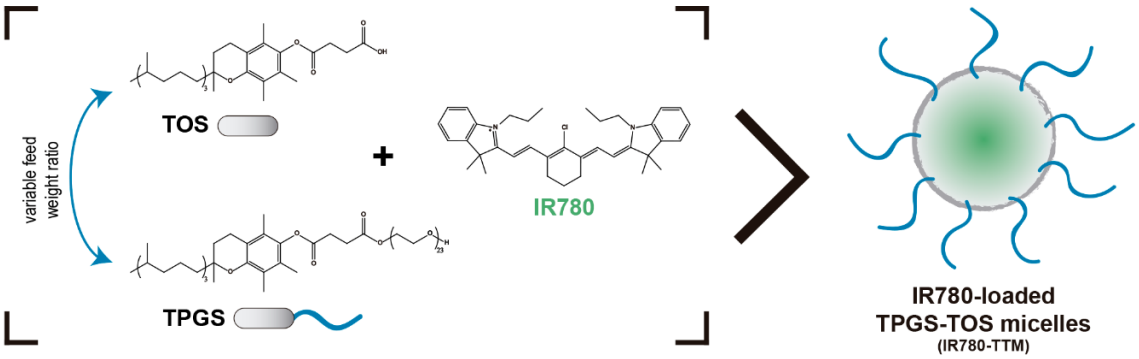

Figure 11. Schematic illustration of the protocol used to produce IR780-loaded TPGS-TOS micelles. Micelles encapsulating IR780 were prepared using different feed weight ratios of TPGS:TOS.

Aims

The main objective of this masters' thesis was to develop a vitamin E-based micellar nanocarrier to deliver a NIR photoabsorber to breast cancer cells and subsequently evaluate the effect of NIR irradiation in these cells.

The specific aims of this thesis comprise the:

- → Preparation of IR780-loaded TPGS-TOS micelles;
- → Characterization and modulation of micelles' physicochemical properties;
- → Investigation of micelles' ability to absorb NIR light and photothermal efficiency under NIR laser irradiation;
- → Evaluation of IR780-loaded TPGS-TOS micelles biocompatibility;
- → Assessment of micelles capacity to be internalized in breast cancer cells;
- → Evaluation of IR780-loaded micelles therapeutic effect under NIR laser irradiation in breast cancer cells.

Chapter 2
Experimental Section

2. Experimental Section

2.1. Materials

Dulbecco's Modified Eagle's Medium F-12 (DMEM-F12), IR780, resazurin, TOS, TPGS, trypsin and 2',7'-dichlorofluorescein diacetate (H_2DCF-DA) were acquired from Sigma–Aldrich (Sintra, Portugal). Michigan Cancer Foundation-7 (MCF-7; ATCC® HTB-22™) cell line was purchased from ATCC (Middlesex, United Kingdom). Fetal bovine serum (FBS) was obtained from Biochrom AG (Berlin, Germany). Cell culture plates and T-flasks were acquired from Orange Scientific (Braine-l'Alleud, Belgium) and cell imaging plates were purchased from Ibidi GmbH (Munich, Germany).

2.2. Methods

2.2.1. Production of IR780-TTM

IR780-TTM were produced by using the nanoprecipitation technique as previously described by Duhem *et al.*, with slight modifications (Duhem *et al.*, 2014a). First, a 1 mL acetone solution containing 250 µg of IR780 and 5 mg of different weight feed ratios of TPGS:TOS was prepared (**Table 1**). This solution was then added dropwise to 5 mL of double deionized water (0.22 µm filtered, 18.2 MΩ·cm) under constant magnetic stirring for 1 h at room temperature (RT). Afterward, the aqueous solution was dialyzed (1000 Da molecular weight cut-off) for 2 h at RT, yielding IR780-TTM. Samples from three different batches (n = 3) were analyzed and each sample was screened three times (three measurements per n). Blank micelles were prepared according to the above described procedure but without adding IR780.

Table 1. Formulation conditions used for preparing IR780-TTM.

Sample abbreviation	TPGS feed (%)	TPGS feed (mg)	TOS feed (mg)	IR780 feed (µg)
IR780-100TTM	100	5	0	250
IR780-67TTM	67	3.33	1.67	250
IR780-60TTM	60	3	2	250
IR780-50TTM	50	2.5	2.5	250
IR780-40TTM	40	2	3	250
IR780-33TTM	33	1.67	3.33	250
IR780-25TTM	25	1.25	3.75	250
IR780-0TTM	0	0	5	250

2.2.2. Physicochemical characterization of IR780-TTM

Size distribution and zeta potential of TTM were determined by dynamic light scattering in a Zetasizer Nano ZS (Malvern Instruments Ltd., Worcestershire, United Kingdom), at 25 °C, through the detection of scattered light at a 173° angle. Micelles' morphology was characterized by Transmission Electron Microscopy (TEM). For this analysis, particles samples were stained with phosphotungstic acid and immediately placed onto formvar-coated copper grids. Samples were left to dry at RT and then were analyzed in a Hitachi-HT7700 transmission electron microscope (Hitachi Ltd., Tokyo, Japan), operated at an accelerating voltage of 80 kV.

2.2.3. IR780-TTM encapsulation efficiency and loading content

The capacity of TTM to encapsulate IR780 was evaluated by ultraviolet-visible-NIR (UV-vis-NIR) absorption spectroscopy. In brief, the produced micelles were freeze-dried (ScanVac CoolSafe, LaboGene ApS, Lynge, Denmark) and re-suspended in methanol (MetOH) to disrupt the powdered particles. Then, samples absorbance at the wavelength of 781 nm was determined using an Evolution 201 UV-Visible spectrophotometer (Thermo Fisher Scientific Inc., Massachusetts, United States of America) and the concentration of IR780 in each sample was calculated using a calibration curve of IR780 solubilized in MetOH. The EE was defined by the ratio between the determined weight of IR780 encapsulated in the micelles and the total weight of IR780 initially fed during the formulation of micelles (**Equation (1)**). In turn, IR780 loading content (LC) was defined by the ratio between the weight of IR780 encapsulated in the micelles and the total weight of IR780-TTM (**Equation (2)**).

$$EE\ (\%) = \frac{\text{Weight of IR780 encapsulated in micelles}}{\text{Weight of IR780 initially fed}} \times 100 \qquad \textbf{(1)}$$

$$LC\ (\%) = \frac{\text{Weight of IR780 encapsulated in micelles}}{\text{Weight of IR780-TTM}} \times 100 \qquad \textbf{(2)}$$

2.2.4. Phototherapeutic capacity of IR780-TTM

The ability of IR780-TTM to be applied in cancer phototherapy was primarily investigated through the analysis of their absorbance (600 – 900 nm). For this purpose, the absorption spectra of free-IR780 (2 μg mL^{-1}) and IR780-TTM (2 μg mL^{-1} of IR780 equivalents) in water and in MetOH (after freeze-drying) were acquired. The photothermal efficiency of IR780-TTM was assessed *in vitro* through the determination of the temperature variation when samples were exposed to NIR laser irradiation. For this purpose, IR780-TTM loaded with different concentrations of IR780 (20, 10 and 1.5 μg mL^{-1}) were exposed to NIR irradiation (808 nm, 1.7 W cm^{-2}) for 5 min. At each time-point, the temperature was recorded with a thermocouple thermometer. Experiments performed with water were used as control.

2.2.5. Cell culture

MCF-7 cells were cultured in 75 cm^2 T-flasks and incubated in an incubator with controlled temperature (37 °C) and humidified atmosphere (5 % CO_2) with DMEM-F12 medium supplemented with 10 % (v/v) FBS and 1 % streptomycin/gentamycin (v/v). The culture medium was periodically changed to ensure sufficient nutrient supply to the cells. Whenever confluence was reached (80-85 %), cells were harvested by using 0.18 % trypsin (Gaspar *et al.*, 2014).

2.2.6. IC50 determination

The half maximal inhibitory concentration (IC50) of TPGS, TOS, and IR780 for MCF-7 cells was evaluated through the resazurin assay, as previously described by our group (Moreira *et al.*, 2014). In brief, MCF-7 cells were seeded in 96-well plates at a density of 8 x 10^3 cells/well. After 24 h, the culture medium was removed and cells were incubated with fresh medium containing different concentrations of TPGS, TOS or IR780 during 48 h. After this period, the medium was discarded and cells were incubated in the dark with fresh medium containing resazurin (10 % v/v) for 4 h, at 37 °C, in an atmosphere of 5 % CO_2. Then, resorufin fluorescence was quantified at 560/590 nm excitation/emission wavelengths in a Spectramax Gemini EM spectrofluorometer (Molecular Devices LLC, California, United States of America). Non-treated cells were used as negative controls (K^-) and those treated with ethanol (70 %) were used as positive controls (K^+).

2.2.7. Evaluation of IR780-TTM biocompatibility

To determine the biocompatibility of IR780-TTM, a density of 1 x 10^4 MCF-7 cells/well was subcultured in 96-well plates. After 24 h, the medium was discarded and cells were incubated with different concentrations of IR780-TTM re-suspended in medium during 24, 48 and 72 h. Afterward, the cell viability was determined using the resazurin assay as described above. Non-treated cells were used as negative controls (K^-) and those treated with ethanol (70 %) were used as positive controls (K^+).

2.2.8. Assessment of IR780-TTM internalization in cancer cells

The applicability of micelles for cellular imaging and their capacity to be internalized by MCF-7 cells were confirmed by Confocal Laser Scanning Microscopy (CLSM), as previously described elsewhere (Gaspar *et al.*, 2015a). In brief, 2 x 10^4 MCF-7 cells/well were seeded in µ-slide 8-well imaging plates (Ibidi GmbH, Munich, Germany). On the following day, the culture medium was replaced with fresh medium containing free-IR780 (1.5 µg mL^{-1}) or IR780-TTM (1.5 µg mL^{-1} of IR780 equivalents), followed by an incubation of 24 h. Then, cells were fixed in paraformaldehyde 4 % (15 min, RT) and rinsed with phosphate buffered saline (PBS) solution. Imaging experiments were performed in a Zeiss LSM 710 confocal microscope (Carl Zeiss AG, Oberkochen, Germany) using an excitation wavelength of 633 nm and an emission of 700-758 nm. Consecutive Z-Stacks were acquired and consequent image analysis was performed in Zeiss Zen 2011 software.

2.2.9. Evaluation of phototherapy mediated by IR780-TTM

For the evaluation of the *in vitro* phototherapeutic capability of IR780-TTM, MCF-7 cells at a density of 8 x 10^3 cells/well were seeded in 96-well plates. On the following day, the culture medium was removed and cells were incubated with fresh medium containing free-IR780 (1.5 μg mL^{-1}) or IR780-TTM (1.5 μg mL^{-1} of IR780 equivalents) for 24 h. Then, the medium was exchanged with fresh medium and cells were exposed to laser irradiation (808 nm, 1.7 W cm^{-2}) for 5 min, followed by an incubation of 24 h. Afterward, the cell viability was determined using the above described resazurin method. Non-treated cells were used as negative controls (K^-) and those treated with ethanol (70 %) were used as positive controls (K^+).

2.2.10. *In vitro* detection of ROS generation by IR780-TTM

H_2DCF-DA probe was used to analyze the intracellular generation of ROS as previously reported by Wang and co-workers, with slight modifications (Wang *et al.*, 2016). Briefly, MCF-7 cells were seeded on μ-slide 8-well imaging plates (Ibidi GmbH, Munich, Germany) as described above for CLSM analysis. Cells were then incubated with IR780-TTM (1.5 μg mL^{-1} of IR780 equivalents) for 24 h. One hour before laser irradiation, cells were washed twice with PBS and incubated in the dark with 10 μM of H_2DCF-DA (in serum- and phenol red-free culture medium) in the dark at 37 °C, in a 5 % CO_2 atmosphere. After washing the cells twice with PBS, fresh medium (serum- and phenol red-free) was added to each well and cells were exposed to NIR irradiation (808 nm, 1.7 W cm^{-2}) for 5 min. Cells non-irradiated and non-treated with micelles were used as the control group. Subsequently, fluorescence images were immediately acquired in a confocal microscope (Zeiss LSM 710, Carl Zeiss AG, Oberkochen, Germany), using an excitation wavelength of 488 nm and an emission of 493-599 nm. Zeiss Zen 2011 software was used for subsequent image visualization. ImageJ (National Institutes of Health, Maryland, United States of America) was used to determine the mean fluorescence intensity (ten Z-Stacks were analyzed for each condition) (Schneider *et al.*, 2012).

2.2.11. Statistical analysis

The obtained results are represented as the mean ± standard deviation (SD). For assays involving comparison of multiple test groups, one-way analysis of variance (ANOVA) with the Student-Newman-Keuls test was employed. A value of p inferior to 0.05 was considered statistically significant. The statistical analysis of the data was conducted in GraphPad Prism v6.0 software (Trial version, GraphPad Software, California, United States of America).

Chapter 3
Results and Discussion

3. Results and Discussion

3.1. Characterization of IR780-TTM

For the successful use of IR780 in biomedical applications, this molecule must be loaded in nanosized carriers due to its low water solubility (< 0.4 μg mL^{-1}) (Jiang *et al.*, 2015). In this way, TPGS and TOS were selected to prepare micelles that were able to encapsulate and deliver IR780, due to their physicochemical and biological properties (Danhier *et al.*, 2014).

IR780-TTM were prepared using different TPGS:TOS weight feed ratios in order to disclose the formulation conditions that yield micelles with suitable physicochemical characteristics to be applied in cancer therapy (**Table 1**; **Figure 12A**).

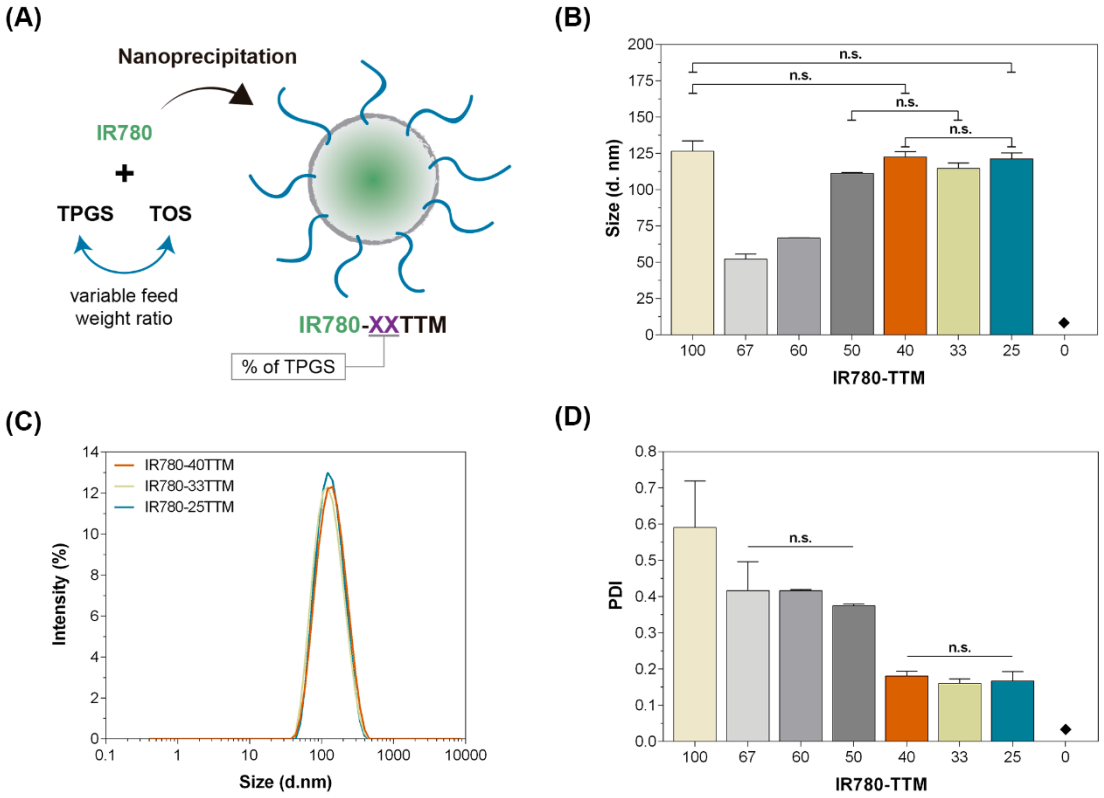

Figure 12. Determination of the size and polydispersity index (PDI) of IR780-TTM (represented in terms of TPGS content (%)). **(A)** Schematic illustration of IR780-TTM formulation process. The physicochemical properties of IR780-TTM were optimized by varying the percentage of TPGS and TOS used in the nanoprecipitation process. **(B)** Size of IR780-TTM and **(C)** representative size distribution of IR780-40TTM, IR780-33TTM and IR780-25TTM. **(D)** PDI of IR780-TTM. Formulation conditions of IR780-0TTM yielded precipitates visible at naked eye (◆). Each bar represents the mean ± SD, samples from three different batches were analyzed (*n* = 3; three measurements per *n*). The differences between the bars not signed with n.s. were statistically significant. n.s. = non significant.

Nanomedicines with sizes comprehended between 100-200 nm are often considered optimal for cancer therapy applications (Blanco *et al.*, 2015; Tan *et al.*, 2014). In this regard, the IR780-TTM prepared with 40, 33 and 25 % of TPGS presented sizes of 123, 115 and 121 nm, respectively, and a narrow size distribution (polydispersity index (PDI) of 0.18 ± 0.01, 0.16 ± 0.01 and 0.17 ± 0.02, respectively), which are within the optimal size range that allow tumor accumulation through the EPR effect (**Figure 12B**-**D**). The other formulations displayed an inappropriate size and/or PDI (**Figure 12B** and **D**). Moreover, our results revealed that micelles prepared only with TPGS presented a high polydispersity, while the sole utilization of TOS produced visible aggregates, which suggest a cooperative interaction between these two vitamin E derivatives in micelles assembly.

Thereby, the IR780-40TTM, IR780-33TTM, and IR780-25TTM were selected for the following studies. Interestingly, the characterization data of blank TTM (**Table 2**) revealed that these have a different size and PDI than their IR780-TTM equivalents. This may indicate that the hydrophobic interactions established between IR780 and the compounds that form the micellar core play an important role in the physicochemical characteristics of the IR780-TTM. Moreover, it should be stressed that the reported results are referred to an average of three measurements of three distinct batches for each formulation, thus revealing the consistency of particle size distribution between batches and demonstrating the reproducibility of the nanoprecipitation method used to assemble IR780-TTM. The selected IR780-TTM displayed an inferior size and lower polydispersity than Dox-loaded TTM (size of 353.7 ± 2.5 nm and PDI of 0.33 ± 0.02) previously reported in the literature, which increases their potential to be used in cancer therapy (Danhier *et al.*, 2014). The IR780-40TTM, IR780-33TTM and IR780-25TTM presented a negative superficial charge (zeta potential of -28.5 ± 1.36, -31.9 ± 0.40 and -29.8 ± 1.53 mV, respectively), which is in agreement with that previously reported for TPGS-based nanomaterials (de Melo-Diogo *et al.*, 2014; Zeng *et al.*, 2013; Zhang *et al.*, 2015).

Table 2. Size and PDI values of blank TTM. Formulations prepared solely with TOS yielded precipitates visible at naked eye (◆). Data are presented as mean ± SD.

TPGS content (%)	Blank TTM	
	Size (d.nm)	PDI
100	94.1 ± 1.3	0.272 ± 0.002
67	74.6 ± 1.7	0.355 ± 0.035
60	157.9 ± 1.6	0.289 ± 0.005
50	244.6 ± 2.1	0.363 ± 0.028
40	233.4 ± 0.6	0.253 ± 0.012
33	203.8 ± 0.7	0.253 ± 0.036
25	133.4 ± 1.7	0.138 ± 0.013
0	◆	◆

In terms of morphology, TEM analysis of IR780-TTM demonstrated that the nanoformulations have a spherical shape (**Figure 13**), which is an important feature since spherical-shaped nanomaterials often display a high tumor uptake as well as an enhanced internalization by cancer cells (Black *et al.*, 2014; Chen *et al.*, 2012; Li *et al.*, 2015).

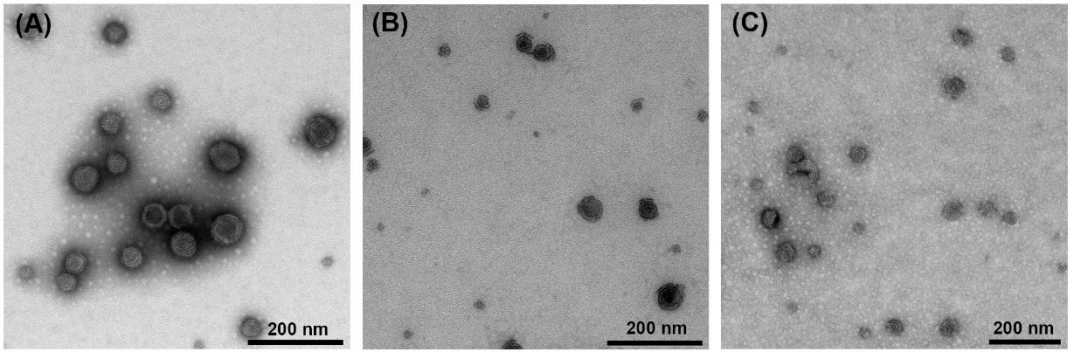

Figure 13. Morphological characterization of IR780-TTM. TEM images of IR780-40TTM **(A)**, IR780-33TTM **(B)** and IR780-25TTM **(C)**.

The IR780-TTM were capable of encapsulating IR780 with high efficiency (> 80 %) (see **Figure 14A** for further details). Such result can be explained by the strong hydrophobic interactions established between IR780 and the TOS-based core of the micelles. Moreover, the encapsulation of IR780 in TTM resulted in a 105- to 115-fold increase in the IR780 solubility, which ensures their applicability in the studies subsequently herein performed. Furthermore, the IR780-40TTM, IR780-33TTM, and IR780-25TTM demonstrated a similar loading capacity (**Figure 14B**). These results are similar to those reported in the literature for polymeric micelles and confirm the excellent capability of TTM as carriers to perform IR780 delivery (de Melo-Diogo *et al.*, 2014; Gaspar *et al.*, 2015a; Kutty *et al.*, 2015; Liang *et al.*, 2015; Wang *et al.*, 2014b).

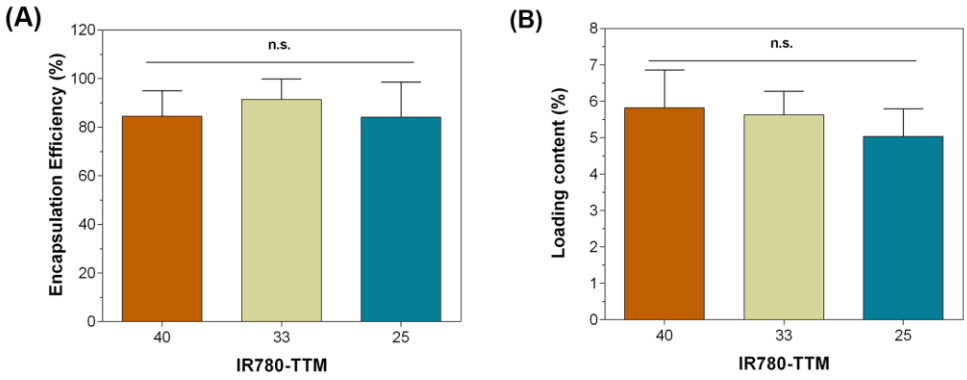

Figure 14. Characterization of IR780 encapsulation efficiency **(A)** and loading content **(B)** in TTM. Each bar represents the mean ± SD, samples from three different batches were analyzed (*n* = 3; three measurements per *n*). n.s. = non significant.

3.2. Phototherapeutic ability of IR780-TTM

In order to characterize the phototherapeutic ability of IR780-TTM, the UV-vis-NIR absorption spectra of IR780-TTM and free-IR780 were acquired (**Figure 15**). IR780 in its free form (dissolved in MetOH) presented a maximum absorption peak at 781 nm, while when encapsulated in TTM its absorption peak has a red-shift (λ_{max} = 800 nm) (**Figure 15A**), which might be attributed to changes in solvent polarity or to hydrophobic interactions of this compound with micelles' core (Jiang *et al.*, 2015). To further confirm this hypothesis, UV-vis-NIR absorption spectra of powdered IR780-TTM dissolved in MetOH were also acquired and, as expected, the bathochromic shift of IR780 was not present (**Figure 15B**). As can be observed in **Figure 15A** inset, the absorbance of the IR780-TTM at the wavelength of 808 nm is about 2.4-times higher than that of free-IR780 in that same wavelength. Since an 808 nm laser will be employed in the *in vitro* experiments, this increased absorption of the IR780-TTM at 808 nm is of extreme importance since it is expected to enhance light-NPs interactions, and consequently increase the cytotoxicity generated by NPs upon laser irradiation. Moreover, the application of NIR light in phototherapies is highly desirable due to its deep penetration in biological tissues and low absorption by off-target components (Rwei *et al.*, 2015).

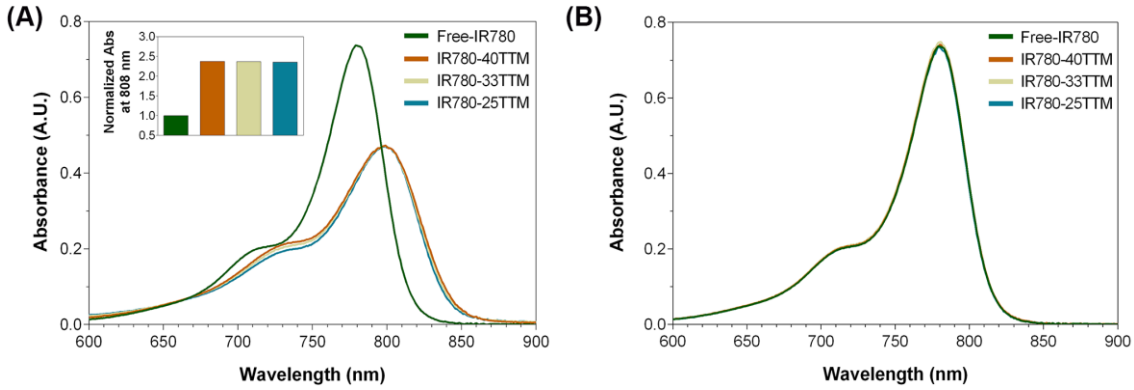

Figure 15. Evaluation of IR780-TTM NIR absorption capacity. **(A)** UV-vis-NIR absorption spectra and absorption at 808 nm (inset) of IR780-TTM (in water) normalized to the absorption of free-IR780 dissolved in MetOH at the same wavelength. **(B)** UV-vis-NIR absorption spectra of IR780-TTM and free-IR780 both re-suspended in MetOH. The concentration of IR780 used in the experiments was 2 μg mL^{-1}.

The applicability of IR780-TTM as PTT agents was assessed by recording the temperature variation upon laser irradiation (**Figure 16**). In general, the temperature increased quickly in the first 2 min of irradiation and decreased gradually during the remaining time. This behavior may be attributed to the photodegradation of IR780 by NIR light as suggested by Yuan and co-workers (Yuan *et al.*, 2015). Importantly, the photodegradation products of IR780-based nanomaterials are biocompatible, which further amplifies the therapeutic potential of the IR780-TTM (Yuan *et al.*, 2015). IR780-40TTM, IR780-33TTM, and IR780-25TTM demonstrated a similar heating profile under NIR laser irradiation, which suggests that the differences in the composition and in the physicochemical characteristics of IR780-TTM do not influence their PTT ability. For the lowest concentration of IR780-TTM tested (1.5 μg mL^{-1} of IR780 equivalents), the temperature variation ($\Delta T < 2$ °C) under NIR laser irradiation was similar to that occurring

in the control (water), which suggests that this dose is not capable of inducing damage to cancer cells (**Figure 16**). In contrast, IR780-TTM loaded with 10 and 20 μg mL^{-1} of IR780 triggered a temperature increase of about 11 °C and 18 °C, respectively (**Figure 16**), under NIR light irradiation, that is concomitant with hyperthermic cell damage (generally attained for temperatures above 42 °C). Hence, at specific concentrations, IR780-TTM may be explored as PTT agents. For instance, Han *et al.* prepared IR780-loaded poly(2-methacryloyloxyethyl phosphorylcholine)-*b*-poly(*n*-butylmethacrylate) (PMPC-*b*-PBMA) NPs, that at a concentration of 40 μg mL^{-1} of IR780, produced under NIR laser irradiation a maximum temperature variation of 10 °C (Han *et al.*, 2015). Herein, the IR780-TTM produced a similar photoinduced heat using only a concentration of 10 μg mL^{-1} of IR780. The enhanced photothermal capacity of IR780-TTM may be correlated with their improved NIR absorption, thereby confirming their potential for cancer PTT.

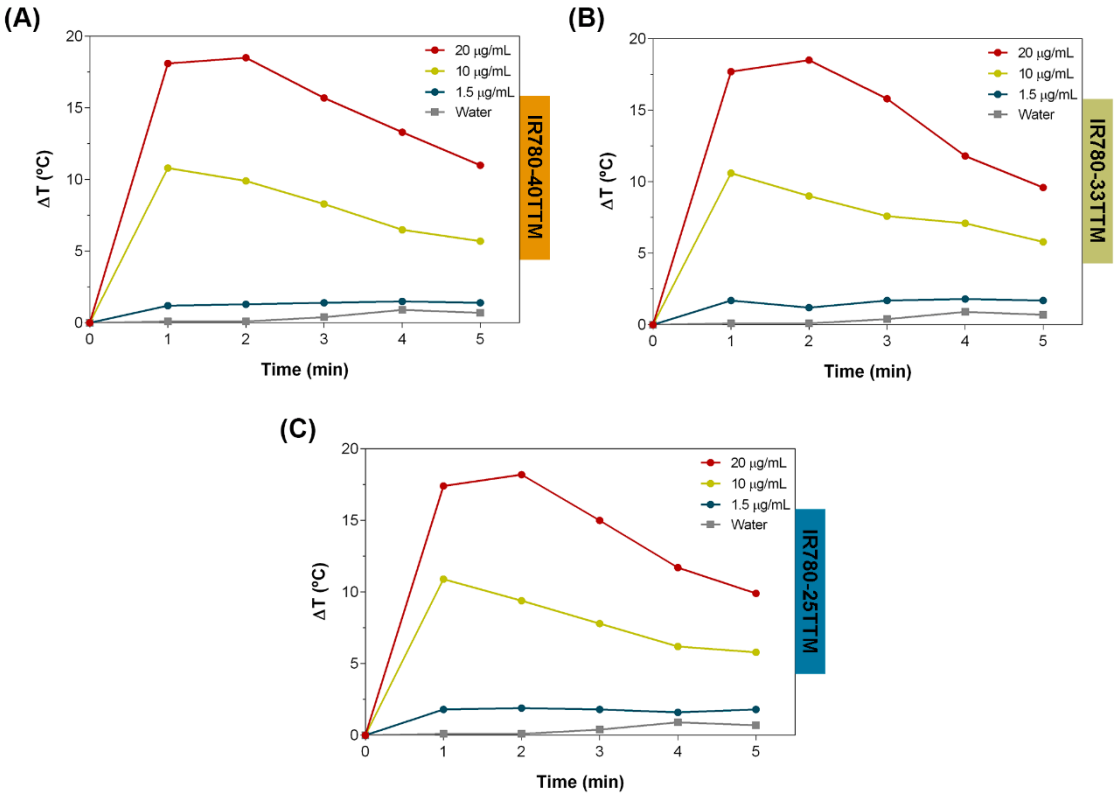

Figure 16. Determination of temperature variations induced by IR780-TTM at different concentrations (in water) over 5 min of NIR irradiation (808 nm, 1.7 W cm^{-2}). Water was used as control.

3.3. IC50 determination and evaluation of IR780-TTM biocompatibility

The IC50 of TPGS, TOS, and IR780 in MCF-7 cells was first determined in order to assess the sensibility of the breast cancer cell line to these compounds and also to confirm their intrinsic anticancer activity. The obtained IC50 values were 8.46, 35.86 and 15.61 μM for TPGS, TOS, and IR780, respectively (**Figure 17**), which are slightly inferior to those previously reported in literature (Abd-El Fattah *et al.*, 2012; Neophytou *et al.*, 2014; Wang *et al.*, 2014a). In fact,

TPGS and TOS have intrinsic anticancer activity, through diverse mechanisms involving: (i) deregulation of the levels of anti-apoptotic proteins, (ii) activation of pro-apoptotic signaling pathways and (iii) generation of ROS (Constantinou *et al.*, 2008; Neophytou *et al.*, 2014; Youk *et al.*, 2005). Furthermore, it was recently proposed that the anticancer activity of IR780 may involve the disruption of mitochondrial functions (Wang *et al.*, 2014a).

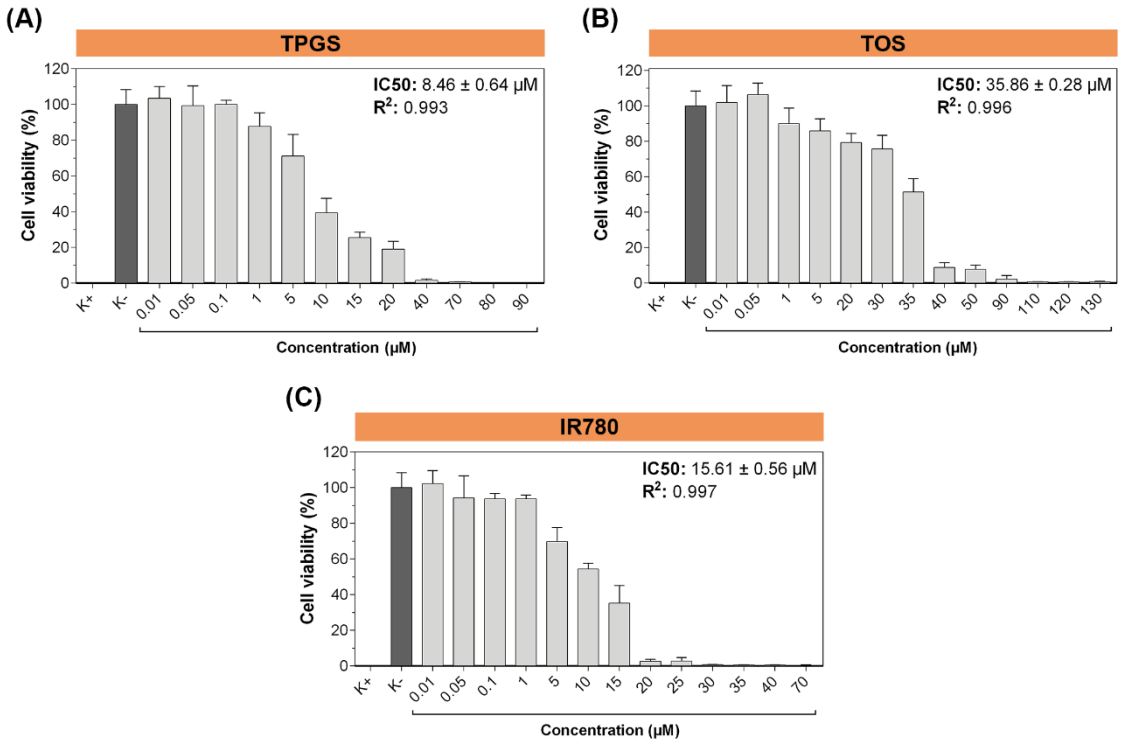

Figure 17. Determination of the IC50 value of TPGS **(A)**, TOS **(B)** and IR780 **(C)** in MCF-7 cells after 48 h incubation. K^- is the negative control (live cells) and K^+ the positive control (dead cells). Each bar represents the mean ± SD (*n* = 5).

Afterward, the biocompatibility of the IR780-TTM was evaluated using MCF-7 as a model cell line. The IR780-TTM did not induce alterations in cell metabolism at concentrations up to 40 µg mL^{-1}, suggesting their biocompatibility up to this dosage (**Figure 18**). For higher concentrations of IR780-TTM, the cell metabolism was severely affected. Such effect is likely to occur as a consequence of the intrinsic anticancer activity of both vitamin E derivatives that form the TTM and suggests that the micelles may be employed to trigger cancer cells death at higher concentrations. As a matter of fact, this concept was recently demonstrated by Palao-Suay and co-workers, which verified that NPs loaded with TOS can be applied for anticancer therapy (Palao-Suay *et al.*, 2016). Therefore, the vitamin E-based composition of IR780-TTM opens the possibility for these micelles to be applied in the future as anticancer agents or to explore drug-vitamin E synergistic effects.

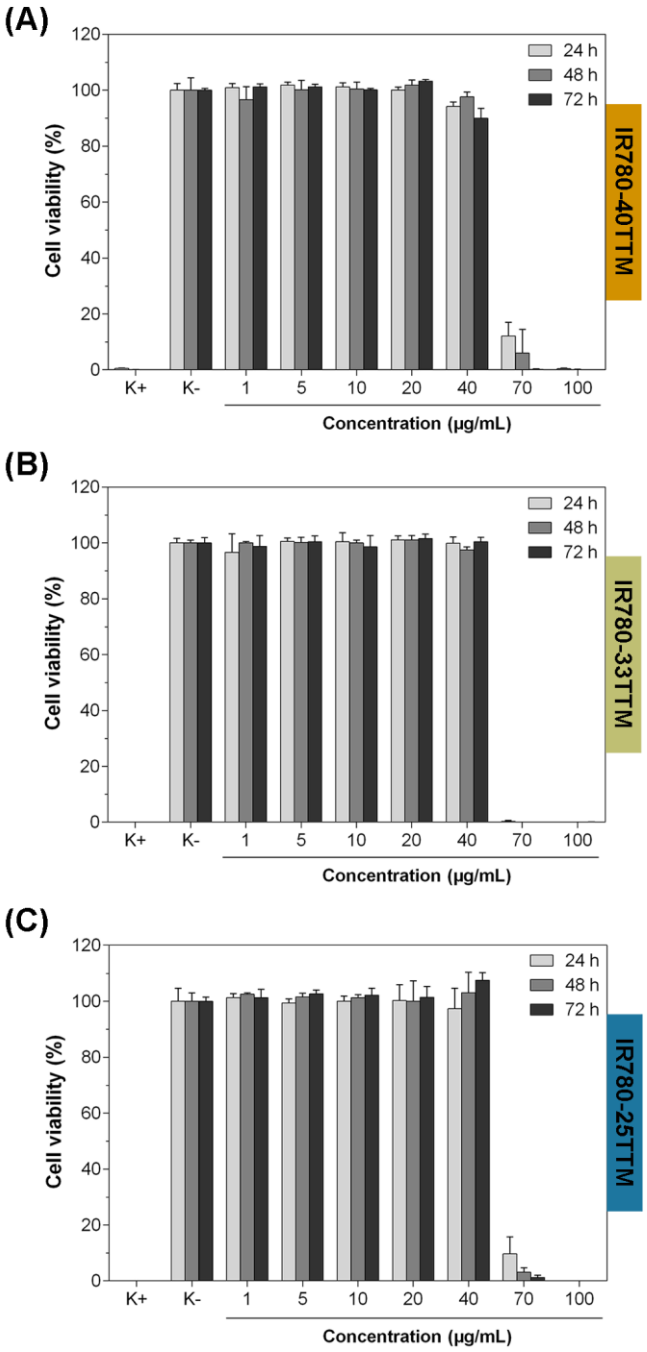

Figure 18. Evaluation of the biocompatibility of IR780-40TTM **(A)**, IR780-33TTM **(B)** and IR780-25TTM **(C)**, using MCF-7 as model cell line at different concentrations (ranging from 1 to 100 µg mL^{-1}) and different incubation times (24, 48 and 72 h). K^- is the negative control (live cells) and K^+ the positive control (dead cells). Each bar represents the mean ± SD (n = 5).

3.4. Cellular internalization of IR780-TTM

IR780-TTM must be internalized by cancer cells in order for them to be used in cancer phototherapy. Therefore, CLSM images were acquired to assess IR780-TTM uptake by MCF-7 cells. The different IR780-TTM formulations were able to enter into cells after 24 h of incubation (**Figure 19**). In contrast, cells incubated with free-IR780 had almost no fluorescence signals, which suggests a poor uptake of free-IR780 by MCF-7 cells and emphasizes the crucial role of TTM in IR780 internalization in cells. In previous studies, it was already reported that

TPGS-coated materials have an improved internalization in cancer cells and an enhanced biological performance (Gaspar *et al.*, 2015b; Kulkarni and Feng, 2013; Wang *et al.*, 2014b; Win and Feng, 2005). Moreover, TPGS-based NPs with a size of 100 nm exhibit a higher cellular uptake efficiency than those with a size of 25, 50, 200 and 500 nm (Kulkarni and Feng, 2013). Therefore, these reports suggest that the IR780-TTM, which have sizes comprehended between 115 and 123 nm, present optimal characteristics to be internalized by cells. Importantly, CLSM assays also demonstrated that IR780-TTM can be used for cancer cell imaging and that may be explored in future works for *in vivo* tumor imaging.

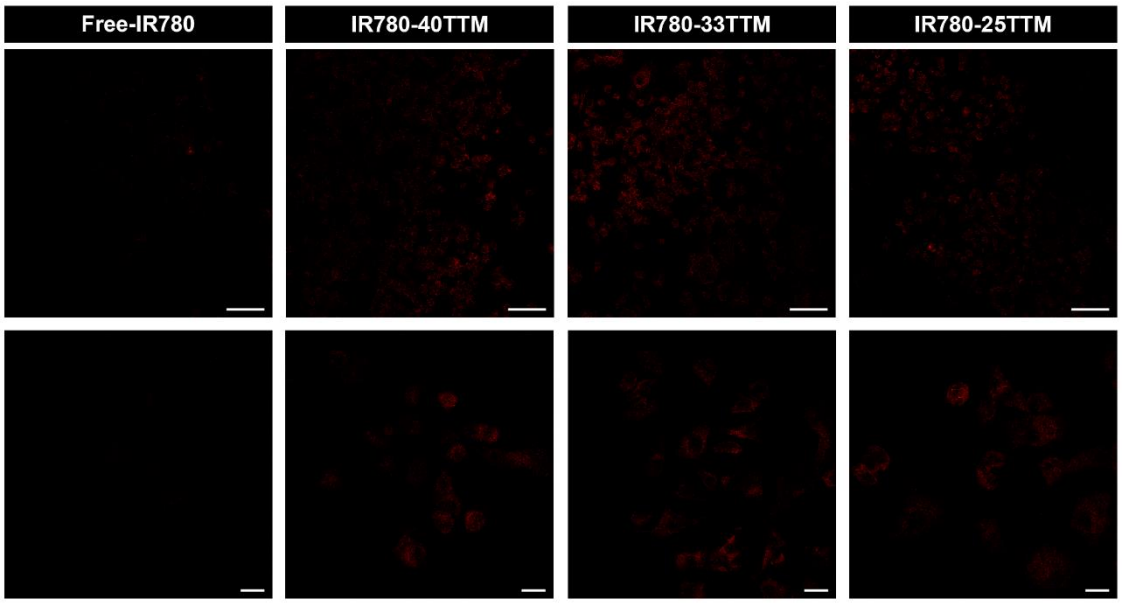

Figure 19. Representative CLSM images of free-IR780 and IR780-TTM internalization in MCF-7 cells after 24 h of incubation. Scale bar of images in the upper row is 100 μm and in the bottom row is 20 μm.

3.5. Phototherapy mediated by IR780-TTM

The photoinduced cytotoxic effect of IR780-TTM micelles towards MCF-7 cells was evaluated by exposing cells to micelles, followed by NIR laser irradiation (**Figure 20A**). For this assay, cells were incubated with a biocompatible concentration of IR780-TTM (below 40 μg mL^{-1}) to guarantee that the therapeutic effect mediated by the micelles upon NIR laser irradiation is related to the photoinduced cytotoxicity of the loaded IR780 and will not be masked by the micellar nanocarrier itself. As shown in **Figure 20B**, the combination of NIR light with IR780-40TTM or IR780-33TTM induced a decrease in cells viability (80 % on average). The application of IR780-25TTM and NIR light produced a slightly lower therapeutic effect since cells viability decreased by ≈ 66 % (**Figure 20B**). Cells exposed to free-IR780 and NIR light remained viable, which suggests that the poor uptake of free-IR780 by cancer cells (**Figure 19**) impairs its therapeutic application and stresses the importance of IR780 encapsulation in TTM for cancer phototherapy. Importantly, the application of the NIR light *per se* did not induce any alterations in cells viability (**Figure 20B**). Moreover, cells treated with non-irradiated free-IR780 or non-irradiated IR780-TTM also displayed a high viability (**Figure 20B**). Taken together, these results

demonstrate that IR780-TTM have the potential to be used as an on-demand anticancer treatment since these only induce cytotoxicity to cancer cells upon NIR laser irradiation.

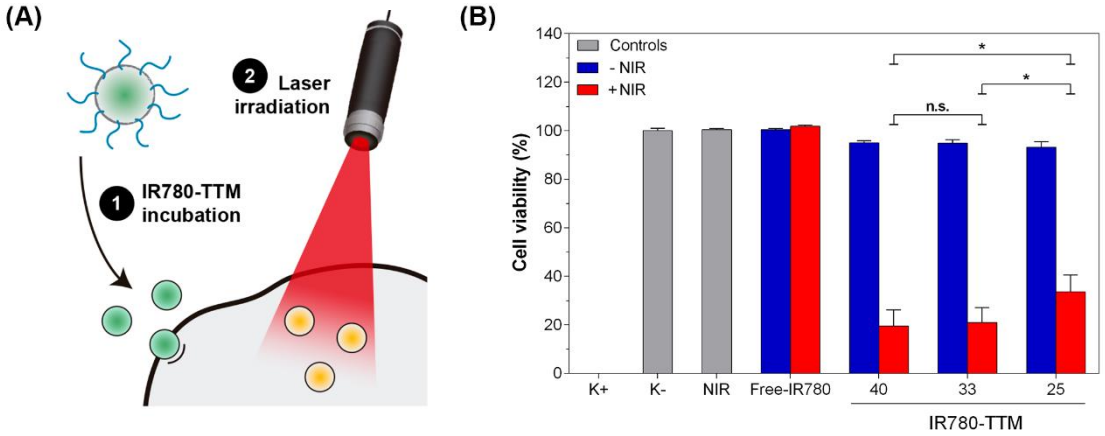

Figure 20. Breast cancer phototherapy mediated by IR780-TTM. **(A)** Schematic of the procedure used in this study. **(B)** Evaluation of the phototherapeutic effect mediated by IR780-TTM (1.5 μg mL^{-1} of IR780 equivalents) and free-IR780 (1.5 μg mL^{-1}) in MCF-7 cells without (- NIR) and with (+ NIR) laser irradiation (808 nm, 1.7 W cm^{-2}, 5 min). K^- is the negative control (live cells); NIR represents cells treated solely with NIR irradiation; K^+ is the positive control (dead cells). Each bar represents the mean ± SD (n = 5), * p < 0.05, n.s. = non significant.

According to the *in vitro* photothermal assays (**Figure 16**), the IR780-TTM at the tested concentration (1.5 μg mL^{-1} of IR780 equivalents) did not induce any cell death due to temperature increase. Therefore, we hypothesized that the photoinduced cytotoxicity of IR780-TTM could be mediated by ROS since IR780 has also been described as being capable of producing these reactive molecules upon NIR irradiation (Bazylińska *et al.*, 2014; Cheng *et al.*, 2015; Jiang *et al.*, 2015). Such hypothesis was then investigated by performing H_2DCF-DA assays to detect the intracellular generation of general ROS (**Figure 21A**). In this assay, the fluorescence signal emerging from this probe is proportional to the intracellular oxidative stress. As observed in **Figure 21B**, cells treated with IR780-TTM and NIR light had 1.29- to 1.38-fold higher mean fluorescence intensity than non-treated cells (control – **Figure 21B**). Based on these observations, the generation of ROS by IR780-TTM upon NIR laser irradiation is likely to be the main mechanism that induces cellular death. Such is also supported by the cell viability results (**Figure 20B**), since from the three formulations exposed to NIR light, the IR780-25TTM produced a slightly lower therapeutic effect which is in agreement with their lower production of ROS (**Figure 21B**). Another important finding of the H_2DCF-DA assay was the fact that cells treated with IR780-TTM (non-irradiated) displayed 1.11- to 1.19-fold increased mean fluorescence intensity when compared to the control (**Figure 21B**). Such result is explained by the TPGS and TOS intrinsic capacity to generate ROS, which may also give an important contribution to the outcome of the PDT mediated by the IR780-TTM.

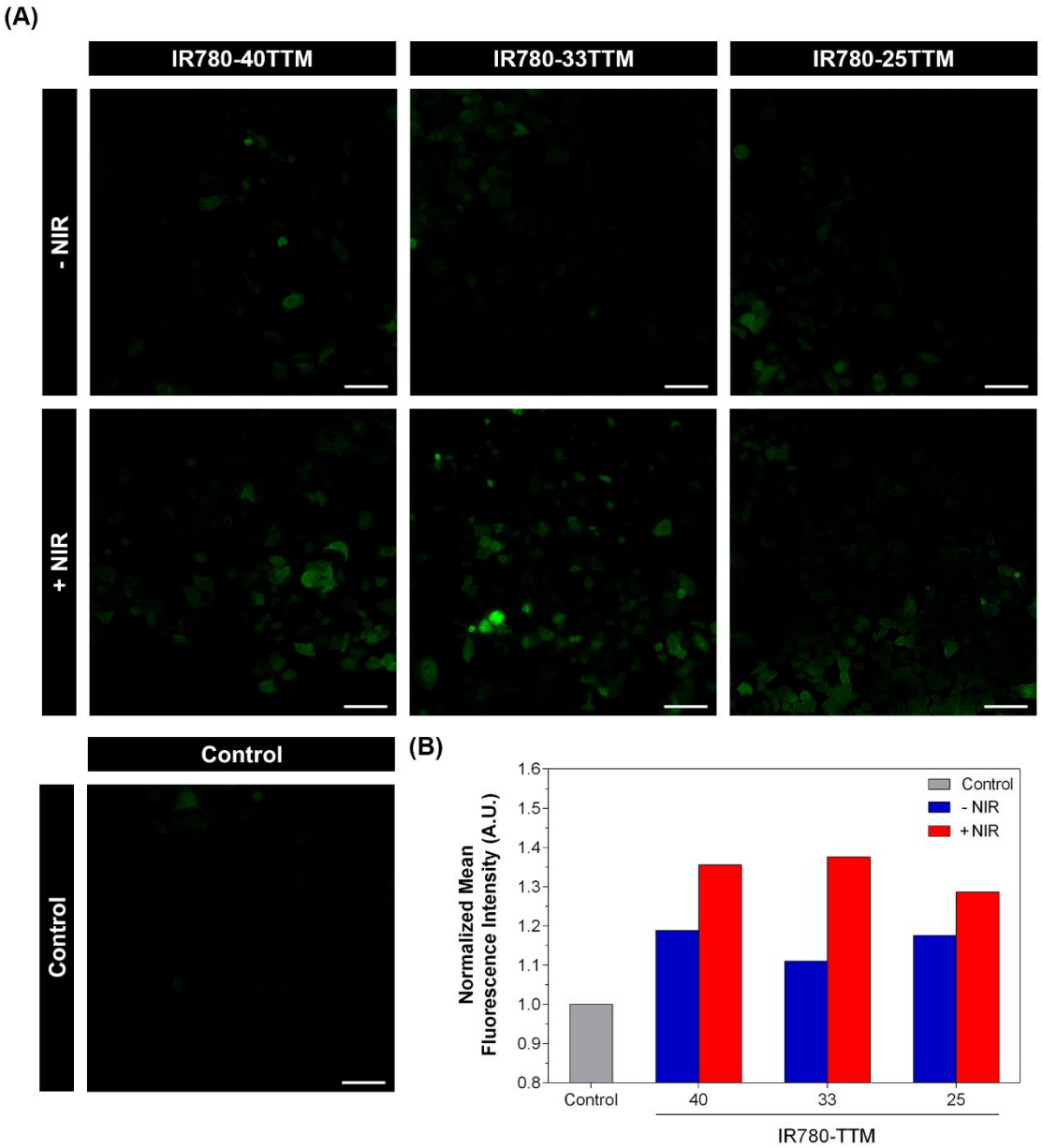

Figure 21. Photodynamic effect mediated by IR780-TTM. **(A)** Representative CLSM images of the H_2DCF-DA assay and **(B)** quantitative analysis of the ROS generated after exposition of MCF-7 cells to IR780-TTM (1.5 μg mL^{-1} of IR780 equivalents) without (- NIR) and with (+ NIR) laser irradiation (808 nm, 1.7 W cm^{-2}, 5 min). Cells incubated solely with H_2DCF-DA were the control group. The scale bar is 100 μm.

In our experiments, the phototherapeutic effect mediated by IR780-TTM was achieved using a lower concentration of IR780 (1.5 μg mL^{-1}) than the other IR780-loaded NPs reported so far in literature for cancer PTT and PDT (**Table 3**), such as (i) micellar and polymer-based NPs (Chen *et al.*, 2016; Han *et al.*, 2015; Li *et al.*, 2016; Peng *et al.*, 2011), (ii) tumor-targeted NPs (Jiang *et al.*, 2015; Wang *et al.*, 2016; Yue *et al.*, 2013), and (iii) NPs capable to develop oxygen self-enriched PDT (Cheng *et al.*, 2015). This fact also attests for the phototherapeutic potential of the IR780-TTM, whose effectiveness is likely owed to their (i) suitable physicochemical properties, (ii) improved NIR absorption and (iii) PDT enhanced by vitamin E derivatives ROS production.

Overall, the obtained results revealed that IR780-TTM are a multimodal system (PDT, PTT and fluorescence imaging) that can be investigated in future works for image-guided cancer phototherapy. Moreover, the application of vitamin E derivatives in cancer PDT is also a promising approach worth of further investigation.

Table 3. Summary of the different IR780-loaded NPs produced for cancer phototherapy.

Sample	[IR780] (μg mL^{-1})	NIR irradiation parameters	Cell line	Cell viability[1] (%)	Mechanism of action	Ref.
IR780-loaded mPEG[a)]-*b*-PCL micelles	10	808 nm, 0.6 W cm^{-2}, 20 min	HCT-116[b)]	15	PTT	(Peng *et al.*, 2011)
HF[c)]-IR780 NPs	5	808 nm, 0.6 W cm^{-2}, 5 min	MCF-7	16	PTT	(Yue *et al.*, 2013)
IR780-loaded Perfluorocarbon nanodroplets	2.09	808 nm, 2 W cm^{-2}, 20 sec	MCF-7	18	PDT	(Cheng *et al.*, 2015)
	8.35		CT-26[d)]	11		
PMPC-*b*-PBMA/ IR780 NPs	40	808 nm, 0.5 W cm^{-2}, 1 min	HepG2[e)]	25	PTT	(Han *et al.*, 2015)
HSA[f)]-IR780 NPs	3.13	808 nm, 1 W cm^{-2}, 5 min	MCF-7	18	PTT and PDT	(Jiang *et al.*, 2015)
PMDPC[g)]-IR780 micelles	5	808 nm, 0.8 W cm^{-2}, 5 min	BxPC-3[h)]	16	PTT	(Chen *et al.*, 2016)
IR780-loaded PBMA-*b*-PMPC micelles	2.6	808 nm, 1.5 W cm^{-2}, 5 min	MCF-7/ ADR[i)]	59.4	PTT	(Li *et al.*, 2016)
Tf[j)]-IR780 NPs	3.85	808 nm, 1 W cm^{-2}, 5 min	CT-26	24.4	PTT and PDT	(Wang *et al.*, 2016)
IR780-TTM	1.5	808 nm, 1.7 W cm^{-2}, 5 min	MCF-7	20	PDT	**this thesis**

[1] approximated value; [a)] methoxy poly(ethylene glycol); [b)] human colon carcinoma cell line; [c)] heparin-folic acid; [d)] murine colon adenocarcinoma cell line; [e)] human hepatocyte carcinoma cell line; [f)] human serum albumin; [g)] poly(12-methacryloyloxy dodecyl phosphorylcholine); [h)] human primary pancreatic adenocarcinoma cell line; [i)] adriamycin-resistant; [j)] transferrin.

Chapter 4

Conclusions and Future Perspectives

4. Conclusions and Future Perspectives

Cancer incidence and mortality continues to grow and, despite the limitless efforts that have been made, there is no effective cure available for this disease yet. In fact, the currently available treatments have an unsatisfactory performance mainly due to their side effects and drug resistance. To surpass these problems, the scientific community has been pursuing the development of new therapeutic strategies. Particularly, light-induced treatments based on the application of NIR photoabsorbers offer the possibility of fine-tuning the therapeutic intervention over time. However, these treatments still lack selectivity towards the tumor tissue and are hindered by the poor solubility of the light-responsive molecules. In this way, the delivery of NIR photoabsorbers using nanosized carriers is a promising approach to improve the bioavailability of the entrapped compounds within the tumor and mediate an effective therapeutic effect in response to NIR laser irradiation.

In this thesis, the delivery of IR780 (NIR photoabsorber) in TPGS-TOS micelles (IR780-TTM) was studied for breast cancer phototherapy. During micelles formulation, the utilization of specific TPGS:TOS weight feed ratios yielded IR780-TTM with appropriate physicochemical properties to benefit from the EPR effect. Moreover, IR780-TTM were able to encapsulate IR780 with high efficiency, which is crucial to overcome the poor solubility of this molecule. The strong absorption of IR780-TTM in the NIR region and their good photothermal efficiency under NIR laser irradiation confirmed the capacity of IR780-TTM to act as photothermal agent. In addition, cellular uptake experiments showed that IR780-TTM are internalized by MCF-7, which is crucial to ensure that the full potential of this phototherapy can be achieved. The cellular internalization of micelles was visualized by taking advantage of the intrinsic fluorescence of IR780 and such confirmed the potential of IR780-TTM for cancer cell imaging. Furthermore, cytotoxicity studies revealed that IR780-TTM induce the ablation of cancer cells after being irradiated with NIR light, through the generation of ROS (PDT). Moreover, it was verified that TPGS and TOS may contribute to such effect since these two vitamin E derivatives can generate these reactive molecules. One of the main achievements of this thesis was the lowest concentration of IR780 reported so far in literature, that is able to produce a photoinduced cytotoxicity.

Overall, the IR780-TTM developed in this thesis present optimal characteristics to be used as ultra-effective multimodal systems for breast cancer cells phototherapy (PDT and PTT) and imaging. In the future, the versatility of IR780-TTM opens the possibility for these micelles to be explored for *in vivo* image-guided phototherapy of breast cancer. Moreover, the investigation of drug-vitamin E synergistic effects and the application of vitamin E derivatives in cancer PDT are also promising approaches worth of further investigation.

Chapter 5
Bibliographic References

5. Bibliographic References

Abd-El Fattah, A. A., Darwish, H. A., Fathy, N., Raafat, A., and Shouman, S. A. (2012). *Promising antitumor effect of alpha-tocopheryl succinate in human colon and liver cancer cells*. Medicinal Chemistry Research, 21: 2735-2743.

Aggarwal, P., Hall, J. B., McLeland, C. B., Dobrovolskaia, M. A., and McNeil, S. E. (2009). *Nanoparticle interaction with plasma proteins as it relates to particle biodistribution, biocompatibility and therapeutic efficacy*. Advanced Drug Delivery Reviews, 61: 428-437.

Al-Jamal, W. T., and Kostarelos, K. (2011). *Liposomes: from a clinically established drug delivery system to a nanoparticle platform for theranostic nanomedicine*. Accounts of Chemical Research, 44: 1094-1104.

Barcellos-Hoff, M. H., Lyden, D., and Wang, T. C. (2013). *The evolution of the cancer niche during multistage carcinogenesis*. Nature Reviews Cancer, 13: 511-518.

Barz, M., Luxenhofer, R., Zentel, R., and Vicent, M. J. (2011). *Overcoming the PEG-addiction: well-defined alternatives to PEG, from structure–property relationships to better defined therapeutics*. Polymer Chemistry, 2: 1900-1918.

Bazylińska, U., Lewińska, A., Lamch, Ł., and Wilk, K. A. (2014). *Polymeric nanocapsules and nanospheres for encapsulation and long sustained release of hydrophobic cyanine-type photosensitizer*. Colloids and Surfaces A: Physicochemical and Engineering Aspects, 442: 42-49.

Bertrand, N., Wu, J., Xu, X., Kamaly, N., and Farokhzad, O. C. (2014). *Cancer nanotechnology: the impact of passive and active targeting in the era of modern cancer biology*. Advanced Drug Delivery Reviews, 66: 2-25.

Black, K. C., Wang, Y., Luehmann, H. P., Cai, X., Xing, W., Pang, B., Zhao, Y., Cutler, C. S., Wang, L. V., Liu, Y., and Xia, Y. (2014). *Radioactive ^{198}Au-doped nanostructures with different shapes for in vivo analyses of their biodistribution, tumor uptake, and intratumoral distribution*. ACS Nano, 8: 4385-4394.

Blanco, E., and Ferrari, M. (2014). *Emerging nanotherapeutic strategies in breast cancer*. The Breast, 23: 10-18.

Blanco, E., Shen, H., and Ferrari, M. (2015). *Principles of nanoparticle design for overcoming biological barriers to drug delivery*. Nature Biotechnology, 33: 941-951.

Caino, M. C., Meshki, J., and Kazanietz, M. G. (2009). *Hallmarks for senescence in carcinogenesis: novel signaling players*. Apoptosis, 14: 392-408.

Canel, M., Serrels, A., Frame, M. C., and Brunton, V. G. (2013). *E-cadherin–integrin crosstalk in cancer invasion and metastasis*. Journal of Cell Science, 126: 393-401.

Chaffer, C. L., and Weinberg, R. A. (2011). *A perspective on cancer cell metastasis*. Science, 331: 1559-1564.

Chen, T., Guo, X., Liu, X., Shi, S., Wang, J., Shi, C., Qian, Z., and Zhou, S. (2012). *A strategy in the design of micellar shape for cancer therapy*. Advanced Healthcare Materials, 1: 214-224.

Chen, Y., Li, Z., Wang, H., Wang, Y., Han, H., Jin, Q., and Ji, J. (2016). *IR-780 loaded phospholipid mimicking homopolymeric micelles for near-IR imaging and photothermal therapy of pancreatic cancer*. ACS Applied Materials & Interfaces, 8: 6852-6858.

Cheng, L., Wang, C., Feng, L., Yang, K., and Liu, Z. (2014). *Functional nanomaterials for phototherapies of cancer*. Chemical Reviews, 114: 10869-10939.

Cheng, Y., Cheng, H., Jiang, C., Qiu, X., Wang, K., Huan, W., Yuan, A., Wu, J., and Hu, Y. (2015). *Perfluorocarbon nanoparticles enhance reactive oxygen levels and tumour growth inhibition in photodynamic therapy*. Nature Communications, 6: 8785-8792.

Cheng, Y., and Xu, T. (2008). *The effect of dendrimers on the pharmacodynamic and pharmacokinetic behaviors of non-covalently or covalently attached drugs*. European Journal of Medicinal Chemistry, 43: 2291-2297.

Chu, K. F., and Dupuy, D. E. (2014). *Thermal ablation of tumours: biological mechanisms and advances in therapy*. Nature Reviews Cancer, 14: 199-208.

Colditz, G. A., Bohlke, K., and Berkey, C. S. (2014). *Breast cancer risk accumulation starts early: prevention must also*. Breast Cancer Research and Treatment, 145: 567-579.

Collnot, E.-M., Baldes, C., Wempe, M. F., Kappl, R., Hüttermann, J., Hyatt, J. A., Edgar, K. J., Schaefer, U. F., and Lehr, C.-M. (2007). *Mechanism of inhibition of P-glycoprotein mediated efflux by vitamin E TPGS: influence on ATPase activity and membrane fluidity*. Molecular Pharmaceutics, 4: 465-474.

Constantinou, C., Papas, A., and Constantinou, A. I. (2008). *Vitamin E and cancer: an insight into the anticancer activities of vitamin E isomers and analogs*. International Journal of Cancer, 123: 739-752.

Danhier, F., Feron, O., and Préat, V. (2010). *To exploit the tumor microenvironment: passive and active tumor targeting of nanocarriers for anti-cancer drug delivery*. Journal of Controlled Release, 148: 135-146.

Danhier, F., Kouhé, T. T. B., Duhem, N., Ucakar, B., Staub, A., Draoui, N., Feron, O., and Préat, V. (2014). *Vitamin E-based micelles enhance the anticancer activity of doxorubicin*. International Journal of Pharmaceutics, 476: 9-15.

de Melo-Diogo, D., Gaspar, V. M., Costa, E. C., Moreira, A. F., Oppolzer, D., Gallardo, E., and Correia, I. J. (2014). *Combinatorial delivery of Crizotinib–Palbociclib–Sildenafil using TPGS-PLA micelles for improved cancer treatment*. European Journal of Pharmaceutics and Biopharmaceutics, 88: 718-729.

DeSantis, C. E., Lin, C. C., Mariotto, A. B., Siegel, R. L., Stein, K. D., Kramer, J. L., Alteri, R., Robbins, A. S., and Jemal, A. (2014). *Cancer treatment and survivorship statistics, 2014*. CA: A Cancer Journal for Clinicians, 64: 252-271.

Di Fiore, R., D'Anneo, A., Tesoriere, G., and Vento, R. (2013). *RB1 in cancer: different mechanisms of RB1 inactivation and alterations of pRb pathway in tumorigenesis*. Journal of Cellular Physiology, 228: 1676-1687.

Dolmans, D. E. J. G. J., Fukumura, D., and Jain, R. K. (2003). *Photodynamic therapy for cancer*. Nature Reviews Cancer, 3: 380-387.

Duhem, N., Danhier, F., Pourcelle, V., Schumers, J.-M., Bertrand, O., LeDuff, C. S., Hoeppener, S., Schubert, U. S., Gohy, J.-F., Marchand-Brynaert, J., and Préat, V. (2014a). *Self-assembling doxorubicin–tocopherol succinate prodrug as a new drug delivery system: synthesis, characterization, and in vitro and in vivo Anticancer Activity*. Bioconjugate Chemistry, 25: 72-81.

Duhem, N., Danhier, F., and Préat, V. (2014b). *Vitamin E-based nanomedicines for anti-cancer drug delivery*. Journal of Controlled Release, 182: 33-44.

Ernsting, M. J., Murakami, M., Roy, A., and Li, S.-D. (2013). *Factors controlling the pharmacokinetics, biodistribution and intratumoral penetration of nanoparticles*. Journal of Controlled Release, 172: 782-794.

Etheridge, M. L., Campbell, S. A., Erdman, A. G., Haynes, C. L., Wolf, S. M., and McCullough, J. (2013). *The big picture on nanomedicine: the state of investigational and approved nanomedicine products*. Nanomedicine: Nanotechnology, Biology and Medicine, 9: 1-14.

Farokhzad, O. C., and Langer, R. (2009). *Impact of nanotechnology on drug delivery*. ACS Nano, 3: 16-20.

Ferlay, J., Soerjomataram, I., Dikshit, R., Eser, S., Mathers, C., Rebelo, M., Parkin, D. M., Forman, D., and Bray, F. (2015). *Cancer incidence and mortality worldwide: sources, methods and major patterns in GLOBOCAN 2012*. International Journal of Cancer, 136: E359-E386.

Ferrari, M. (2005). *Cancer nanotechnology: opportunities and challenges*. Nature Reviews Cancer, 5: 161-171.

Fitzmaurice, C., Dicker, D., Pain, A., Hamavid, H., Moradi-Lakeh, M., MacIntyre, M. F., Allen, C., Hansen, G., Woodbrook, R., Wolfe, C., Hamadeh, R. R., Moore, A., Werdecker, A., Gessner, B. D., Te Ao, B., McMahon, B., Karimkhani, C., Yu, C., Cooke, G. S., Schwebel, D. C., Carpenter, D. O., Pereira, D. M., Nash, D., Kazi, D. S., De Leo, D., Plass, D., Ukwaja, K. N., Thurston, G. D., Yun Jin, K., Simard, E. P., Mills, E., Park, E. K., Catala-Lopez, F., deVeber, G., Gotay, C., Khan, G., Hosgood, H. D., 3rd, Santos, I. S., Leasher, J. L., Singh, J., Leigh, J., Jonas, J. B., Sanabria, J., Beardsley, J., Jacobsen, K. H., Takahashi, K., Franklin, R. C., Ronfani, L., Montico, M., Naldi, L., Tonelli, M., Geleijnse, J., Petzold, M., Shrime, M. G., Younis, M., Yonemoto, N., Breitborde, N., Yip, P., Pourmalek, F., Lotufo, P. A., Esteghamati, A., Hankey, G. J., Ali, R., Lunevicius, R., Malekzadeh, R., Dellavalle, R., Weintraub, R., Lucas, R., Hay, R., Rojas-Rueda, D., Westerman, R., Sepanlou, S. G., Nolte, S., Patten, S., Weichenthal, S., Abera, S. F., Fereshtehnejad, S. M., Shiue, I., Driscoll, T., Vasankari, T., Alsharif, U., Rahimi-Movaghar, V., Vlassov, V. V., Marcenes, W. S., Mekonnen, W., Melaku, Y. A., Yano, Y., Artaman, A., Campos, I., MacLachlan, J., Mueller, U., Kim, D., Trillini, M., Eshrati, B., Williams, H. C., Shibuya, K., Dandona, R., Murthy, K., Cowie, B., Amare, A. T., Antonio, C. A., Castaneda-Orjuela, C., van Gool, C. H., Violante, F., Oh, I. H., Deribe, K., Soreide, K., Knibbs, L., Kereselidze, M., Green, M., Cardenas, R., Roy, N., Tillmann, T., Li, Y., Krueger, H., Monasta, L., Dey, S., Sheikhbahaei, S., Hafezi-Nejad, N., Kumar, G. A., Sreeramareddy, C. T., Dandona, L., Wang, H., Vollset, S. E., Mokdad, A., Salomon, J. A., Lozano, R., Vos, T., Forouzanfar, M., Lopez, A., Murray, C., and Naghavi, M. (2015). *The global burden of cancer 2013*. JAMA Oncology, 1: 505-527.

Gaspar, V. M., Baril, P., Costa, E. C., de Melo-Diogo, D., Foucher, F., Queiroz, J. A., Sousa, F., Pichon, C., and Correia, I. J. (2015a). *Bioreducible poly (2-ethyl-2-oxazoline)-PLA-PEI-SS*

triblock copolymer micelles for co-delivery of DNA minicircles and Doxorubicin. Journal of Controlled Release, 213: 175-191.

Gaspar, V. M., Gonçalves, C., de Melo-Diogo, D., Costa, E. C., Queiroz, J. A., Pichon, C., Sousa, F., and Correia, I. J. (2014). *Poly (2-ethyl-2-oxazoline)-PLA-g-PEI amphiphilic triblock micelles for co-delivery of minicircle DNA and chemotherapeutics*. Journal of Controlled Release, 189: 90-104.

Gaspar, V. M., Moreira, A. F., Costa, E. C., Queiroz, J. A., Sousa, F., Pichon, C., and Correia, I. J. (2015b). *Gas-generating TPGS-PLGA microspheres loaded with nanoparticles (NIMPS) for co-delivery of minicircle DNA and anti-tumoral drugs*. Colloids and Surfaces B: Biointerfaces, 134: 287-294.

Giampazolias, E., and Tait, S. W. (2015). *Mitochondria and the hallmarks of cancer*. FEBS Journal, 283: 803-814.

Gillies, R. J., Verduzco, D., and Gatenby, R. A. (2012). *Evolutionary dynamics of carcinogenesis and why targeted therapy does not work*. Nature Reviews Cancer, 12: 487-493.

Gong, J., Chen, M., Zheng, Y., Wang, S., and Wang, Y. (2012). *Polymeric micelles drug delivery system in oncology*. Journal of Controlled Release, 159: 312-323.

Han, H., Zhang, S., Wang, Y., Chen, T., Jin, Q., Chen, Y., Li, Z., and Ji, J. (2015). *Biomimetic drug nanocarriers prepared by miniemulsion polymerization for near-infrared imaging and photothermal therapy*. Polymer, 82: 255-261.

Hanahan, D., and Coussens, L. M. (2012). *Accessories to the crime: functions of cells recruited to the tumor microenvironment*. Cancer Cell, 21: 309-322.

Hanahan, D., and Weinberg, R. A. (2000). *The hallmarks of cancer*. Cell, 100: 57-70.

Hanahan, D., and Weinberg, R. A. (2011). *Hallmarks of cancer: the next generation*. Cell, 144: 646-674.

Hillaireau, H., and Couvreur, P. (2009). *Nanocarriers' entry into the cell: relevance to drug delivery*. Cellular and Molecular Life Sciences, 66: 2873-2896.

Huggett, M. T., Jermyn, M., Gillams, A., Illing, R., Mosse, S., Novelli, M., Kent, E., Bown, S. G., Hasan, T., Pogue, B. W., and Pereira, S. P. (2014). *Phase I/II study of verteporfin photodynamic therapy in locally advanced pancreatic cancer*. British Journal of Cancer, 110: 1698-1704.

Jain, R. K., and Stylianopoulos, T. (2010). *Delivering nanomedicine to solid tumors*. Nature Reviews Clinical Oncology, 7: 653-664.

Jaque, D., Maestro, L. M., Del Rosal, B., Haro-Gonzalez, P., Benayas, A., Plaza, J., Rodriguez, E. M., and Sole, J. G. (2014). *Nanoparticles for photothermal therapies*. Nanoscale, 6: 9494-9530.

Jia, F., Liu, X., Li, L., Mallapragada, S., Narasimhan, B., and Wang, Q. (2013). *Multifunctional nanoparticles for targeted delivery of immune activating and cancer therapeutic agents*. Journal of Controlled Release, 172: 1020-1034.

Jiang, C., Cheng, H., Yuan, A., Tang, X., Wu, J., and Hu, Y. (2015). *Hydrophobic IR780 encapsulated in biodegradable human serum albumin nanoparticles for photothermal and photodynamic therapy*. Acta Biomaterialia, 14: 61-69.

Jones, M.-C., and Leroux, J.-C. (1999). *Polymeric micelles-a new generation of colloidal drug carriers*. European Journal of Pharmaceutics and Biopharmaceutics, 48: 101-111.

Junttila, M. R., and de Sauvage, F. J. (2013). *Influence of tumour micro-environment heterogeneity on therapeutic response*. Nature, 501: 346-354.

Kaur, P., Aliru, M. L., Chadha, A. S., Asea, A., and Krishnan, S. (2016). *Hyperthermia using nanoparticles-Promises and pitfalls*. International Journal of Hyperthermia, 32: 76-88.

Kedar, U., Phutane, P., Shidhaye, S., and Kadam, V. (2010). *Advances in polymeric micelles for drug delivery and tumor targeting*. Nanomedicine: Nanotechnology, Biology and Medicine, 6: 714-729.

Kelly, P. N., and Strasser, A. (2011). *The role of Bcl-2 and its pro-survival relatives in tumourigenesis and cancer therapy*. Cell Death and Differentiation, 18: 1414-1424.

Kim, H., Chung, K., Lee, S., Kim, D. H., and Lee, H. (2016). *Near-infrared light-responsive nanomaterials for cancer theranostics*. Wiley Interdisciplinary Reviews: Nanomedicine and Nanobiotechnology, 8: 23-45.

Knop, K., Hoogenboom, R., Fischer, D., and Schubert, U. S. (2010). *Poly (ethylene glycol) in drug delivery: pros and cons as well as potential alternatives*. Angewandte Chemie International Edition, 49: 6288-6308.

Kulkarni, S. A., and Feng, S.-S. (2013). *Effects of particle size and surface modification on cellular uptake and biodistribution of polymeric nanoparticles for drug delivery*. Pharmaceutical Research, 30: 2512-2522.

Kutty, R. V., and Feng, S.-S. (2013). *Cetuximab conjugated vitamin E TPGS micelles for targeted delivery of docetaxel for treatment of triple negative breast cancers*. Biomaterials, 34: 10160-10171.

Kutty, R. V., Tay, C. Y., Lim, C. S., Feng, S.-S., and Leong, D. T. (2015). *Anti-migratory and increased cytotoxic effects of novel dual drug-loaded complex hybrid micelles in triple negative breast cancer cells*. Nano Research, 8: 2533-2547.

Li, Y., Kröger, M., and Liu, W. K. (2015). *Shape effect in cellular uptake of PEGylated nanoparticles: comparison between sphere, rod, cube and disk*. Nanoscale, 7: 16631-16646.

Li, Z., Wang, H., Chen, Y., Wang, Y., Li, H., Han, H., Chen, T., Jin, Q., and Ji, J. (2016). *pH- and NIR light-responsive polymeric prodrug micelles for hyperthermia-assisted site-specific chemotherapy to reverse drug resistance in cancer treatment*. Small, 12: 2731-2740.

Liang, D., Wang, A.-t., Yang, Z.-z., Liu, Y.-j., and Qi, X.-r. (2015). *Enhance cancer cell recognition and overcome drug resistance using hyaluronic acid and a-tocopheryl succinate based multifunctional nanoparticles*. Molecular Pharmaceutics, 12: 2189-2202.

Lucky, S. S., Soo, K. C., and Zhang, Y. (2015). *Nanoparticles in photodynamic therapy*. Chemical Reviews, 115: 1990-2042.

Luo, D., Carter, K. A., and Lovell, J. F. (2015). *Nanomedical engineering: shaping future nanomedicines*. Wiley Interdisciplinary Reviews: Nanomedicine and Nanobiotechnology, 7: 169-188.

Master, A. M., Qi, Y., Oleinick, N. L., and Gupta, A. S. (2012). *EGFR-mediated intracellular delivery of Pc 4 nanoformulation for targeted photodynamic therapy of cancer: in vitro studies*. Nanomedicine: Nanotechnology, Biology and Medicine, 8: 655-664.

McCarthy, D. J., Malhotra, M., O'Mahony, A. M., Cryan, J. F., and O'Driscoll, C. M. (2015). *Nanoparticles and the blood-brain barrier: Advancing from in-vitro models towards therapeutic significance*. Pharmaceutical Research, 32: 1161-1185.

Miranda, N., Portugal, C., Nogueira, P. J., Farinha, C. S., Oliveira, A. L., Soares, A. P., Alves, M. I., Martins, J., Mendanha, T., Rosa, M. V., Silva, C., and Serra, L. (2015). *Portugal – Doenças Oncológicas em números – 2015*. Lisboa.

Moreira, A. F., Gaspar, V. M., Costa, E. C., de Melo-Diogo, D., Machado, P., Paquete, C. M., and Correia, I. J. (2014). *Preparation of end-capped pH-sensitive mesoporous silica nanocarriers for on-demand drug delivery*. European Journal of Pharmaceutics and Biopharmaceutics, 88: 1012-1025.

Nazir, S., Hussain, T., Ayub, A., Rashid, U., and MacRobert, A. J. (2014). *Nanomaterials in combating cancer: therapeutic applications and developments*. Nanomedicine: Nanotechnology, Biology and Medicine, 10: 19-34.

Nel, A. E., Mädler, L., Velegol, D., Xia, T., Hoek, E. M., Somasundaran, P., Klaessig, F., Castranova, V., and Thompson, M. (2009). *Understanding biophysicochemical interactions at the nano–bio interface*. Nature Materials, 8: 543-557.

Neophytou, C. M., Constantinou, C., Papageorgis, P., and Constantinou, A. I. (2014). *D-alpha-tocopheryl polyethylene glycol succinate (TPGS) induces cell cycle arrest and apoptosis selectively in Survivin-overexpressing breast cancer cells*. Biochemical Pharmacology, 89: 31-42.

Owen, S. C., Chan, D. P., and Shoichet, M. S. (2012). *Polymeric micelle stability*. Nano Today, 7: 53-65.

Palao-Suay, R., Rodrigáñez, L., Aguilar, M. R., Sánchez-Rodríguez, C., Parra, F., Fernández, M., Parra, J., Riestra-Ayora, J., Sanz-Fernández, R., and Román, J. S. (2016). *Mitochondrially Targeted Nanoparticles Based on a-TOS for the Selective Cancer Treatment*. Macromolecular Bioscience, 16: 395-411.

Park, K., Kim, K., Kwon, I. C., Kim, S. K., Lee, S., Lee, D. Y., and Byun, Y. (2004). *Preparation and characterization of self-assembled nanoparticles of heparin-deoxycholic acid conjugates*. Langmuir, 20: 11726-11731.

Pekkanen, A. M., DeWitt, M. R., and Rylander, M. N. (2014). *Nanoparticle enhanced optical imaging and phototherapy of cancer*. Journal of Biomedical Nanotechnology, 10: 1677-1712.

Peng, C.-L., Shih, Y.-H., Lee, P.-C., Hsieh, T. M.-H., Luo, T.-Y., and Shieh, M.-J. (2011). *Multimodal image-guided photothermal therapy mediated by ^{188}Re-labeled micelles containing a cyanine-type photosensitizer*. ACS Nano, 5: 5594-5607.

Petros, R. A., and DeSimone, J. M. (2010). *Strategies in the design of nanoparticles for therapeutic applications*. Nature Reviews Drug Discovery, 9: 615-627.

Pickup, M. W., Mouw, J. K., and Weaver, V. M. (2014). *The extracellular matrix modulates the hallmarks of cancer*. EMBO Reports, 15: 1243-1253.

Pietras, K., and Östman, A. (2010). *Hallmarks of cancer: interactions with the tumor stroma*. Experimental Cell Research, 316: 1324-1331.

Polyak, K. (2007). *Breast cancer: origins and evolution*. The Journal of Clinical Investigation, 117: 3155-3163.

Polyak, K. (2011). *Heterogeneity in breast cancer*. The Journal of Clinical Investigation, 121: 3786–3788.

Rosenholm, J. M., Sahlgren, C., and Lindén, M. (2010). *Towards multifunctional, targeted drug delivery systems using mesoporous silica nanoparticles–opportunities & challenges*. Nanoscale, 2: 1870-1883.

Rudolph, A., Chang-Claude, J., and Schmidt, M. K. (2016). *Gene–environment interaction and risk of breast cancer*. British Journal of Cancer, 114: 125-133.

Runowicz, C. D., Leach, C. R., Henry, N. L., Henry, K. S., Mackey, H. T., Cowens-Alvarado, R. L., Cannady, R. S., Pratt-Chapman, M. L., Edge, S. B., Jacobs, L. A., Hurria, A., Marks, L. B., LaMonte, S. J., Warner, E., Lyman, G. H., and Ganz, P. A. (2016). *American Cancer Society/American Society of Clinical Oncology Breast Cancer Survivorship Care Guideline*. CA: A Cancer Journal for Clinicians, 66: 43-73.

Rwei, A. Y., Wang, W., and Kohane, D. S. (2015). *Photoresponsive nanoparticles for drug delivery*. Nano Today, 10: 451-467.

Saharinen, P., Eklund, L., Pulkki, K., Bono, P., and Alitalo, K. (2011). *VEGF and angiopoietin signaling in tumor angiogenesis and metastasis*. Trends in Molecular Medicine, 17: 347-362.

Schneider, C. A., Rasband, W. S., and Eliceiri, K. W. (2012). *NIH Image to ImageJ: 25 years of image analysis*. Nature Methods, 9: 671-675.

Schroeder, A., Heller, D. A., Winslow, M. M., Dahlman, J. E., Pratt, G. W., Langer, R., Jacks, T., and Anderson, D. G. (2012). *Treating metastatic cancer with nanotechnology*. Nature Reviews Cancer, 12: 39-50.

Siegel, R. L., Miller, K. D., and Jemal, A. (2016). *Cancer statistics, 2016*. CA: A Cancer Journal for Clinicians, 66: 7-30.

Singletary, S. E. (2003). *Rating the risk factors for breast cancer*. Annals of Surgery, 237: 474-482.

Song, X., Chen, Q., and Liu, Z. (2015). *Recent advances in the development of organic photothermal nano-agents*. Nano Research, 8: 340-354.

Stylianopoulos, T., and Jain, R. K. (2015). *Design considerations for nanotherapeutics in oncology*. Nanomedicine: Nanotechnology, Biology and Medicine, 11: 1893-1907.

Sun, T., Zhang, Y. S., Pang, B., Hyun, D. C., Yang, M., and Xia, Y. (2014). *Engineered nanoparticles for drug delivery in cancer therapy*. Angewandte Chemie International Edition, 53: 12320-12364.

Tan, G.-R., Feng, S.-S., and Leong, D. T. (2014). *The reduction of anti-cancer drug antagonism by the spatial protection of drugs with PLA–TPGS nanoparticles*. Biomaterials, 35: 3044-3051.

Tang, Y., Wang, Y., Kiani, M. F., and Wang, B. (2016). *Classification, treatment strategy, and associated drug resistance in breast cancer*. Clinical Breast Cancer, In press.

Thakor, A. S., and Gambhir, S. S. (2013). *Nanooncology: the future of cancer diagnosis and therapy*. CA: A Cancer Journal for Clinicians, 63: 395-418.

Tong, R., and Kohane, D. S. (2012). *Shedding light on nanomedicine*. Wiley Interdisciplinary Reviews: Nanomedicine and Nanobiotechnology, 4: 638-662.

Torre, L. A., Siegel, R. L., Ward, E. M., and Jemal, A. (2016). *Global cancer incidence and mortality rates and trends—an update*. Cancer Epidemiology Biomarkers & Prevention, 25: 16-27.

Trichopoulos, D., Adami, H. O., Ekbom, A., Hsieh, C. C., and Lagiou, P. (2008). *Early life events and conditions and breast cancer risk: from epidemiology to etiology*. International Journal of Cancer, 122: 481-485.

Tryfonidis, K., Senkus, E., Cardoso, M. J., and Cardoso, F. (2015). *Management of locally advanced breast cancer - perspectives and future directions*. Nature Reviews Clinical Oncology, 12: 147-162.

Turner, N., and Grose, R. (2010). *Fibroblast growth factor signalling: from development to cancer*. Nature Reviews Cancer, 10: 116-129.

Twelves, C., Jove, M., Gombos, A., and Awada, A. (2016). *Cytotoxic chemotherapy: Still the mainstay of clinical practice for all subtypes metastatic breast cancer*. Critical Reviews in Oncology/Hematology, 100: 74-87.

Vineis, P., and Wild, C. P. (2014). *Global cancer patterns: causes and prevention*. Lancet, 383: 549-557.

Wang, K., Zhang, Y., Wang, J., Yuan, A., Sun, M., Wu, J., and Hu, Y. (2016). *Self-assembled IR780-loaded transferrin nanoparticles as an imaging, targeting and PDT/PTT agent for cancer therapy*. Scientific Reports, 6: 27421.

Wang, Y., Liu, T., Zhang, E., Luo, S., Tan, X., and Shi, C. (2014a). *Preferential accumulation of the near infrared heptamethine dye IR-780 in the mitochondria of drug-resistant lung cancer cells*. Biomaterials, 35: 4116-4124.

Wang, Z., Wu, Y., Zeng, X., Ma, Y., Liu, J., Tang, X., Gao, Y., Liu, K., Zhang, J., Ming, P., Huang, L., and Mei, L. (2014b). *Antitumor efficiency of D-a-tocopheryl polyethylene glycol 1000 succinate-b-poly (ε-caprolactone-ran-lactide) nanoparticle-based delivery of docetaxel in mice bearing cervical cancer*. Journal of Biomedical Nanotechnology, 10: 1509-1519.

Wicki, A., Witzigmann, D., Balasubramanian, V., and Huwyler, J. (2015). *Nanomedicine in cancer therapy: challenges, opportunities, and clinical applications*. Journal of Controlled Release, 200: 138-157.

Wilk, K. A., Zielinska, K., Pietkiewicz, J., Skolucka, N., Choromanska, A., Rossowska, J., Garbiec, A., and Saczko, J. (2012). *Photo-oxidative action in MCF-7 cancer cells induced by hydrophobic cyanines loaded in biodegradable microemulsion-templated nanocapsules*. International Journal of Oncology, 41: 105-116.

Win, K. Y., and Feng, S.-S. (2005). *Effects of particle size and surface coating on cellular uptake of polymeric nanoparticles for oral delivery of anticancer drugs*. Biomaterials, 26: 2713-2722.

Wissing, S., Kayser, O., and Müller, R. (2004). *Solid lipid nanoparticles for parenteral drug delivery*. Advanced Drug Delivery Reviews, 56: 1257-1272.

Witsch, E., Sela, M., and Yarden, Y. (2010). *Roles for growth factors in cancer progression*. Physiology, 25: 85-101.

Wust, P., Hildebrandt, B., Sreenivasa, G., Rau, B., Gellermann, J., Riess, H., Felix, R., and Schlag, P. (2002). *Hyperthermia in combined treatment of cancer*. Lancet Oncology, 3: 487-497.

Wyld, L., Audisio, R. A., and Poston, G. J. (2015). *The evolution of cancer surgery and future perspectives*. Nature Reviews Clinical Oncology, 12: 115-124.

Xu, X., Farach-Carson, M. C., and Jia, X. (2014). *Three-dimensional in vitro tumor models for cancer research and drug evaluation*. Biotechnology Advances, 32: 1256-1268.

Yilmaz, M., and Christofori, G. (2009). *EMT, the cytoskeleton, and cancer cell invasion*. Cancer and Metastasis Reviews, 28: 15-33.

Youk, H.-J., Lee, E., Choi, M.-K., Lee, Y.-J., Chung, J. H., Kim, S.-H., Lee, C.-H., and Lim, S.-J. (2005). *Enhanced anticancer efficacy of a-tocopheryl succinate by conjugation with polyethylene glycol*. Journal of Controlled Release, 107: 43-52.

Yu, Y., He, Y., Xu, B., He, Z., Zhang, Y., Chen, Y., Yang, Y., Xie, Y., Zheng, Y., and He, G. (2013). *Self-assembled methoxy poly (ethylene glycol)-cholesterol micelles for hydrophobic drug delivery*. Journal of Pharmaceutical Sciences, 102: 1054-1062.

Yuan, A., Qiu, X., Tang, X., Liu, W., Wu, J., and Hu, Y. (2015). *Self-assembled PEG-IR-780-C13 micelle as a targeting, safe and highly-effective photothermal agent for in vivo imaging and cancer therapy*. Biomaterials, 51: 184-193.

Yue, C., Liu, P., Zheng, M., Zhao, P., Wang, Y., Ma, Y., and Cai, L. (2013). *IR-780 dye loaded tumor targeting theranostic nanoparticles for NIR imaging and photothermal therapy*. Biomaterials, 34: 6853-6861.

Zardavas, D., Irrthum, A., Swanton, C., and Piccart, M. (2015). *Clinical management of breast cancer heterogeneity*. Nature Reviews Clinical Oncology, 12: 381-394.

Zeng, X., Tao, W., Mei, L., Huang, L., Tan, C., and Feng, S.-S. (2013). *Cholic acid-functionalized nanoparticles of star-shaped PLGA-vitamin E TPGS copolymer for docetaxel delivery to cervical cancer*. Biomaterials, 34: 6058-6067.

Zhang, C., Wang, S., Xiao, J., Tan, X., Zhu, Y., Su, Y., Cheng, T., and Shi, C. (2010). *Sentinel lymph node mapping by a near-infrared fluorescent heptamethine dye*. Biomaterials, 31: 1911-1917.

Zhang, J., Tao, W., Chen, Y., Chang, D., Wang, T., Zhang, X., Mei, L., Zeng, X., and Huang, L. (2015). *Doxorubicin-loaded star-shaped copolymer PLGA-vitamin E TPGS nanoparticles for lung cancer therapy*. Journal of Materials Science: Materials in Medicine, 26: 1-12.

Zhang, Z., Tan, S., and Feng, S.-S. (2012). *Vitamin E TPGS as a molecular biomaterial for drug delivery*. Biomaterials, 33: 4889-4906.

Zheng, M., Yue, C., Ma, Y., Gong, P., Zhao, P., Zheng, C., Sheng, Z., Zhang, P., Wang, Z., and Cai, L. (2013). *Single-step assembly of DOX/ICG loaded lipid–polymer nanoparticles for highly effective chemo-photothermal combination therapy*. ACS Nano, 7: 2056-2067.